Journal of proteome research

Article

pubs.acs.org/jpr

Senescent Human Fibroblasts Show Increased Glycolysis and Redox Homeostasis with Extracellular Metabolomes That Overlap with Those of Irreparable DNA Damage, Aging, and Disease

Emma L. James,[†] Ryan D. Michalek,[‡] Gayani N. Pitiyage,[†] Alice M. de Castro,[†] Katie S. Vignola,[‡] Janice Jones,[‡] Robert P. Mohney,[‡] Edward D. Karoly,[‡] Stephen S. Prime,[†] and Eric Kenneth Parkinson*[,†,§]

[†]Centre for Clinical & Diagnostic Oral Sciences, Institute of Dentistry, Barts and the London School of Medicine and Dentistry, Queen Mary University of London, Turner Street, London E1 2AD, United Kingdom

[‡]Metabolon, Inc., 617 Davis Drive, Suite 400, Durham, North Carolina 27713, United States

Supporting Information

ABSTRACT: Cellular senescence can modulate various pathologies and is associated with irreparable DNA double-strand breaks (IrrDSBs). Extracellular senescence metabolomes (ESMs) were generated from fibroblasts rendered senescent by proliferative exhaustion (PEsen) or 20 Gy of γ rays (IrrDSBsen) and compared with those of young proliferating cells, confluent cells, quiescent cells, and cells exposed to repairable levels of DNA damage to identify novel noninvasive markers of senescent cells. ESMs of PEsen and IrrDSBsen overlapped and showed increased levels of citrate, molecules involved in oxidative stress, a sterol, monohydroxylipids, tryptophan metabolism, phospholipid, and nucleotide catabolism, as well as reduced levels of dipeptides containing branched chain amino acids. The ESM overlaps with the aging and disease body fluid metabolomes, supporting their utility in the noninvasive detection of human senescent cells in vivo and by implication the detection of a variety of human pathologies. Intracellular metabolites of senescent cells showed a relative increase in glycolysis, gluconeogenesis, the pentose-phosphate pathway, and, consistent with this, pyruvate dehydrogenase kinase transcripts. In contrast, tricarboxylic acid cycle enzyme transcript levels were unchanged and their metabolites were depleted. These results are surprising because glycolysis antagonizes senescence entry but are consistent with established senescent cells entering a state of low oxidative stress.

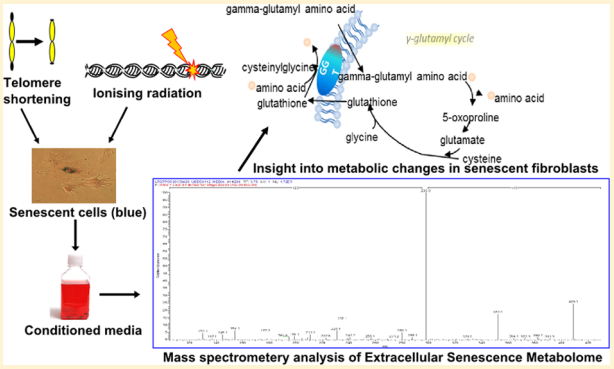

KEYWORDS: *extracellular, senescence, aging, metabolome, DNA damage, energy, redox homeostasis, citrate*

INTRODUCTION

Senescent cells accumulate in aging tissues[1] and in a variety of other human pathologies, including fibrosis,[2] nonhealing wounds,[3] and neoplasia.[4] Furthermore, animal models indicate that senescent cells can modulate these pathologies.[4b,5] Cellular senescence can occur by a variety of mechanisms including telomeric attrition and oncogenic stress,[6] but these mechanisms are thought to converge on the production of DNA double-strand breaks (DSBs), which may result from telomere uncapping[7] or from the generation of oxidative DNA damage and stalled replication forks in the S phase.[8] The failure to repair DSBs (IrrDSBs) leads eventually to the slow accumulation of $p16^{INK4A}$,[9] the formation of senescence-associated heterochromatic foci (SAHF),[10] and permanent cell cycle arrest. Recently, IrrDSBs have been reported to be almost exclusively located at the telomeres,[11] and this may be due to the inability of telomeres to engage efficient DNA end-joining processes.[11a]

Senescent cells can also induce DSBs[12] and senescence[13] in neighboring cells via the secretion of a group of proteins referred to as the senescence-associated secretory phenotype (SASP).[14] Other proteins also accumulate in the serum of late-generation telomerase-deficient mice and provide the potential to detect aging in vivo.[15] The SASP is largely dependent on the establishment of IrrDSBs,[16] but not all of the SASP can be accounted for by known proteins,[14] with accumulating evidence demonstrating regulation of senescence by metabolic enzymes.[17] Furthermore, increased lipid peroxidation and the induction of several SASP proteins are reportedly mediated by the mitochondrial enzyme carnitine palmitoyl transferase 1 in oncogene-induced senescence (OIS) but not following PEsen.[17d]

Metabolomic analysis of aging has been conducted in the body fluids and tissues of several animal models[18] in human twin studies[19] and several other diseases, including neoplasia;[20] however, so far, very little overlap between the body fluid metabolic profiles of the different animal models of aging and

Received: November 27, 2014
Published: February 18, 2015

DOI: 10.1021/pr501221g
J. Proteome Res. 2015, 14, 1854−1871

humans has been reported.[18d,18e,19] Furthermore, the relationship of the previously described in vivo findings to cellular senescence is unclear, as in no instance was senescence or permanent growth arrest investigated. In addition, most of our understanding of the role of metabolism in human cellular senescence, the SASP, and aging has been derived from OIS or neoplasia.[17] There is little information on normal senescence, and there has been no comprehensive analysis of senescence-associated extracellular metabolites and their regulation. In the present study, we show that senescent cells generated by both proliferative exhaustion (PE) and IrrDSBs display an overlapping extracellular metabolic profile that identifies several key pathways that may be useful as noninvasive biomarkers of human aging or cellular senescence cells in vivo. The data also indicate that in vitro human fibroblasts may be useful in investigating the mechanisms underpinning these pathways and thus identify targets for intervention.

EXPERIMENTAL PROCEDURES

Cell Culture

Human fibroblasts were grown in Dulbecco's modified Eagle medium containing 10% vol/vol fetal bovine serum (FBS) in an atmosphere of 10% CO_2/90% air and subcultured once weekly at a density of 1×10^5 cells per 9 cm plate to prohibit confluence. Mean population doublings were calculated as previously described.[21] SA-βGal activity was measured using the senescence detection kit from Biovision.[2] Quiescent control cultures were allowed to remain confluent or in 0.1% vol/vol FBS for 4 days before analysis and the medium changed every day. The PEsen and growing cultures also had the medium changed every day. In some experiments the cells were allowed to remain confluent for 10 days without medium changing. The colon fibroblasts were a generous gift from Professor Chris Paraskeva.

To collect the conditioned medium, we plated cells in T175 flasks or 9 cm dishes in such a way as to ensure a similar cell density to medium volume ratio at day 4, and this never varied by more than 2 fold. The medium was removed, and the cells were washed once with fresh medium before the addition of the appropriate medium. After equilibration in 10% CO_2/90% air, the flasks or dishes were sealed with Parafilm to prevent evaporation and maintain a constant pH while maintaining a high cell-to-medium ratio. Cells were counted at the beginning and the end of the incubation period to obtain an average cell count throughout the collection period. Medium was harvested for analysis after 24 h.

Senescence Induction

Fibroblasts were irradiated in suspension with γ rays from a Cs source at a dose rate of 1.4Gy/min with either 0.5 Gy to induce repairable DNA DSBs or 20 Gy to induce irreparable DNA DSBs, as described, and the cells were left between 0 and 20 days in culture before analysis.

Metabolite Analysis

Conditioned medium was collected after 24 h from the cells and appropriate controls and centrifuged at 800*g* for 2 min, the supernatant was removed and centrifuged again at 13 000 rpm for 2 min, and the final supernatant was snap-frozen on an ethanol−dry-ice bath for 15 min before storage at −80 °C. Unconditioned medium was also prepared identically. Metabolomic profiling analysis was performed by Metabolon as previously described.[22] See the Supplementary Experimental Procedures in the Supporting Information (SI) for details of sample accessioning, sample preparation, ultrahigh performance liquid chromatography/mass spectroscopy, gas chromatography/mass spectroscopy, quality assurance, data extraction, and compound identification. Cell pellets were collected from growing, quiescent, confluent, and PEsen normal human oral fibroblast line 1 (NHOF-1) cells essentially as described.[23] In brief, the cells were rinsed with 0.02% EDTA and incubated with 0.1% trypsin and 0.01% EDTA until they were detached, the trypsin/EDTA solution was neutralized by adding 2× volume of growth medium containing FBS, and the cells were centrifuged at 300*g* for 3 min after an aliquot was taken for counting. The cells were then washed in calcium- and magnesium-free phosphate-buffered saline and centrifuged again before removing the supernatant and freezing the pellet as previously described. The amount of protein in each cell pellet was measured by the Bradford Assay.

Normalization and Data Presentation As Scaled Intensity

For analysis, the median of a given biochemical was determined across all sample groups. This median was subsequently used to scale individual samples to a median of 1 for the group. Identification of known chemical entities was based on comparison with metabolomic library entries of purified standards.[24] Commercially available purified standard compounds have been acquired and registered into LIMS for distribution to both the UPLC−MS/MS and GC−MS platforms[25] for determination of their detectable characteristics. Peaks were quantified using area-under-the-curve. Raw area counts for each metabolite in each sample were normalized to correct for variation resulting from instrument interday tuning differences by the median value for each run-day, therefore setting the medians to 1.0 for each run. This preserved variation between samples but allowed metabolites of widely different raw peak areas to be compared on a similar graphical scale. Rare missing values were given the observed minimum scaled intensity value. These data are graphically presented as scaled intensity and is thus a measure of the relative level of each metabolite in each screen, and data from different screens will have different scaled intensities for the same metabolite. Scaled intensity is thus a relative rather than an absolute measurement. The cell pellet scaled intensities were then further normalized to account for the variation in biomass between different experimental groups and expressed as scaled intensity per unit protein. Because the objective of the extracellular senescence metabolome (ESM) analysis was to detect extracellular markers of senescent cells, regardless of increased biomass, the medium blank-scaled intensity values were subtracted from the ESM-scaled intensity values before being normalized to the average cell number per milliliter of medium. The ESM final results were expressed as net scaled intensity/10^5 cells/mL and were positive when metabolites accumulated and negative when they were depleted.

Statistical Analysis

When appropriate (n = 3 per group), a two-sample t test was used to identify biochemicals that differed significantly between experimental groups. To compare experimental groups across two to five cell lines (n = 6−15), we used the Wilcoxon−Mann−Whitney nonparametric rank test. Pathways were assigned for each metabolite, allowing the examination of overrepresented pathways.

DOI: 10.1021/pr501221g
J. Proteome Res. 2015, 14, 1854−1871

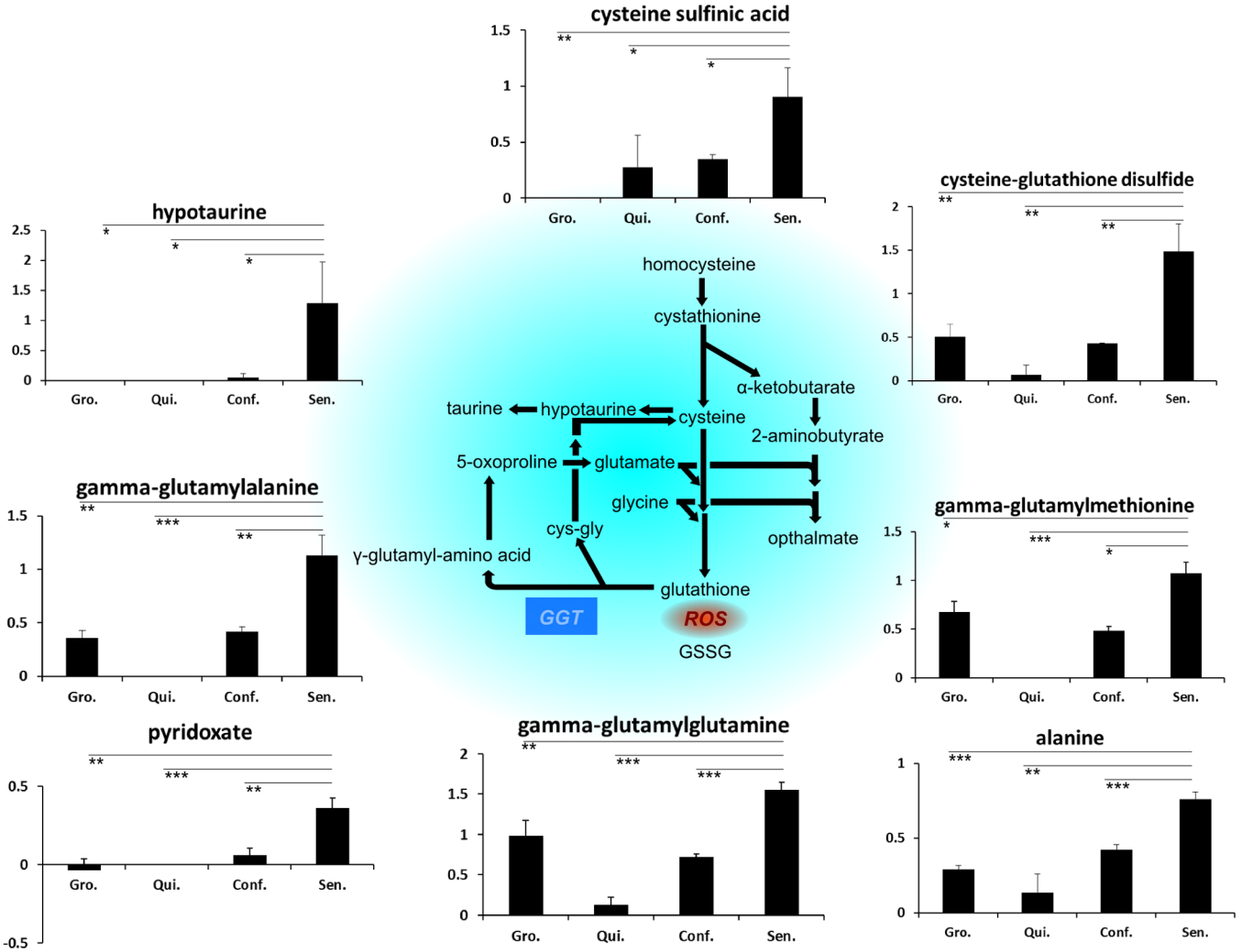

Figure 1. Multiple redox homeostasis metabolites accumulate in the PEsen ESM relative to growing, quiescent and confluent cells. The Figure shows the gamma-glutamyl redox homestasis pathway and net scaled intensity of each metabolite normalized to 1×10^5 cells/mL ± standard deviation in growing (gro.), quiescent (qui.), confluent (conf.), and PEsen (sen.) NHOF-1 oral fibroblasts. $N = 3$ per cell group. The symbols indicate statistically significant results between PEsen cells and all of the other experimental groups and indicate P values as follows: *, $P < 0.05$; **, $P < 0.01$; ***, $P < 0.001$ as assessed by the unpaired two sample t test. GGT, gamma-glutamyl transferase; ROS, reactive oxygen species.

Quantitative Polymerase Chain Reaction Arrays

mRNA was prepared from cells used to generate conditioned media for metabolomics experiments where possible, or from cells cultured under conditions identical to those used for collection of conditioned media, using the RNAeasy mini kit (Qiagen, Manchester, U.K.) with on column DNase digestion; cDNA was prepared using the Qiagen RT2 cDNA synthesis kit. The regulation of glucose metabolism and antioxidant pathways was determined by quantitative polymerase chain reaction (qPCR) using both the Human Glucose Metabolism and Human Oxidative Stress 384-well qPCR arrays from SABiosciences (Qiagen, Manchester, U.K.). Each array contained primers targeting 84 genes known to play important roles in the pathways of interest, in this case glucose metabolism and oxidative stress response. Each array also contained six housekeeping genes, from which we selected the most stable (minimum 2) for use as a reference when calculating the fold up- or down-regulation of a gene in senescent cells compared with a proliferating control. Using Qiagen's suggested data analysis methods we were able to differentiate genuine changes in gene regulation from potential artifacts resulting from low relative expression.

RESULTS

Characterization of the Cultures

Initially, we compared the extracellular metabolites of young proliferating fibroblasts with those that were rendered quiescent by culturing in low serum medium or being held in a confluent state for 4 days (10 days in previous experiments) and the same cells that had undergone senescence by proliferative exhaustion (PEsen) and those that had been induced to senesce by irreparable DNA damage (IrrDSBsen). The cellular senescence status of the cells was confirmed through senescence-associated beta galactosidase (SA-βGal) activity and immunostaining for markers of proliferation (Ki67), DNA damage foci (53BP1), and senescence ($p16^{INK4A}$, see Supplementary Tables S1A and S2 in the SI). As expected, all growth-arrested cells (Supplementary Tables S1 and S2 in the SI) showed a reduction in the percentage of Ki67, but only the PEsen and 10 day confluent cells (Supplementary Tables S1A and S2 in the SI) showed an increase in the percentage of cells with large

DOI: 10.1021/pr501221g
J. Proteome Res. 2015, 14, 1854−1871

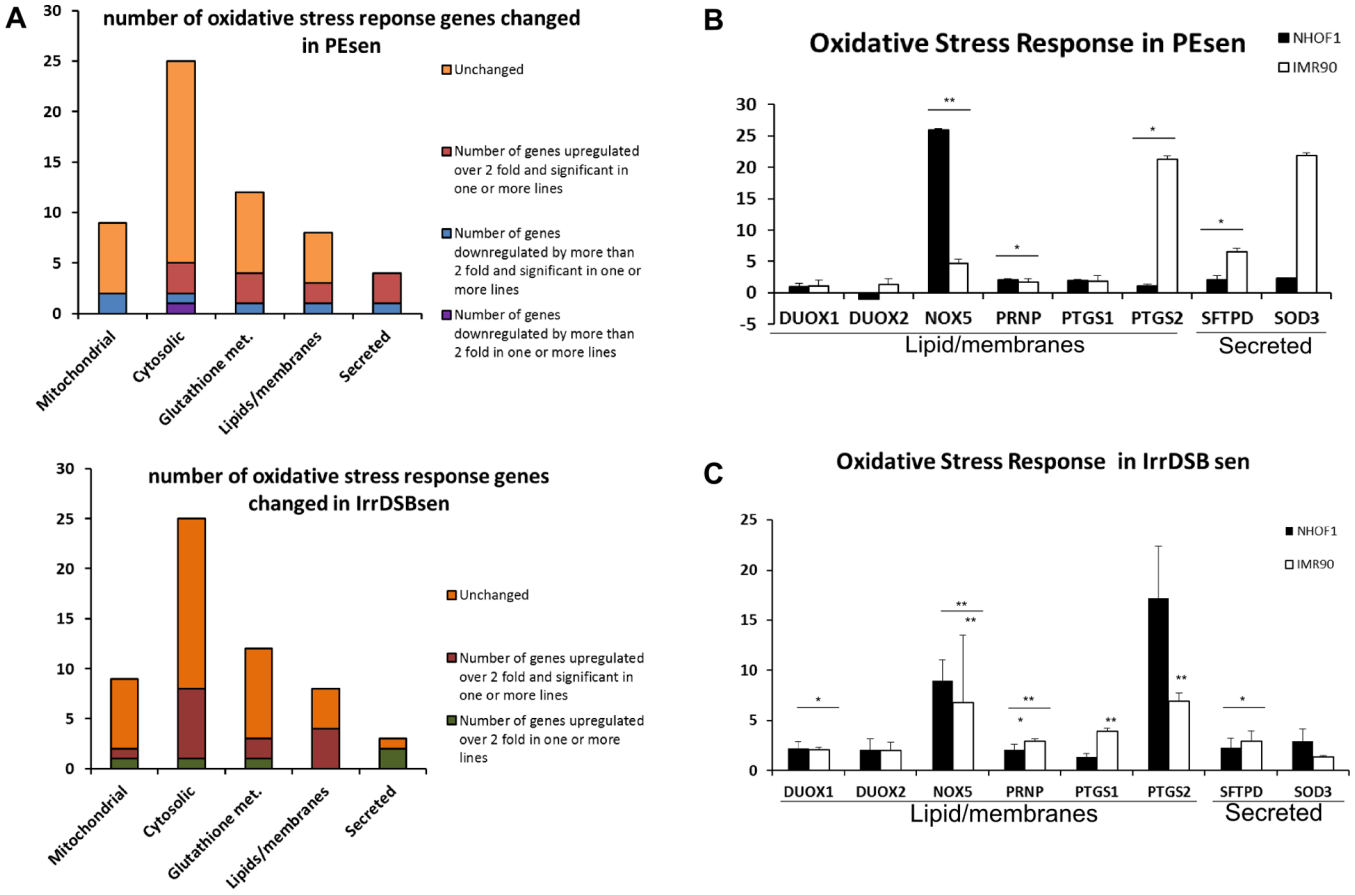

Figure 2. Oxidative damage response enzymes in PEsen and IrrDSBsen are predominantly secreted or involved in lipid membrane, cytosolic and glutathione metabolism. (A) Proportion of enzymes in each pathway transcriptionally altered in PEsen and IrrDSBsen (significant if $p < 0.05$ with Welch's t test). Enzymes statistically altered in one or more cell lines in (B) PEsen and (C) IrrDSBsen as assessed by Welch's t test. *, $P < 0.05$; **, $P < 0.02$. Panel B shows fold change in transcription (y axis) in PEsen. *, $P < 0.05$; **, $P < 0.02$; ***, $P < 0.001$ (Welch's t test). Lines across both bars indicate the level of significance for both cell lines combined. Panel C shows the same data as in panel B but for IrrDSBsen; symbols are the same as those in panel B. $N = 3$ per cell line in each group.

53BP1 foci indicative of irreparable DNA damage,[16] and only PEsen cells showed an increase in $p16^{INK4A}$, which has been proven to be associated with fibroblast senescence in vivo.[2,5f] The percentage of SA-βGal-positive cells ranged from <1% in the growing group to 87.9% in the PEsen group in the NHOF-1 PEsen screen (Supplementary Table S1B in the SI) and 2.4 to 13.2% in the growing group to 43.9−83.1% in the PEsen group in the screen of all five cell lines (Supplementary Table S1B in the SI). Because the colon line showed the highest level of senescence, the results from this line were used to identify ESMs that were relevant to more than one line. The fraction of SA-βGal-positive cells in the IrrDSBsen cultures was generally >90% in all five cell lines studied.

Metabolomic Profiling of Senescent Cell Conditioned Medium

Because metabolites have been implicated in both the regulation of cellular senescence[17a−c] and the SASP,[17d] we conducted metabolomic profiling on the conditioned medium of PEsen NHOF-1 cells and compared the ESMs of these cells with growing counterparts and as controls for reversible growth arrest their quiescent and confluent cultures. We also compared these results with those obtained in a separate screen of five lines of PEsen fibroblasts, including colon fibroblasts versus their growing controls to identify the most robust markers of PEsen (Supplementary Table S3 in the SI). Because four of the lines in this previous screen (including NHOF-1) had fairly low percentage of SA-βGal-positive cells, only four metabolites showed a consistent alteration across all five lines (citrate, 2-hydroxystearate, 3-ureidoproprionate, and glycylvaline), and two others (1-stearoylglycerophosphoinositol and valylaspartate) showed a strong trend (Supplementary Table S4 in the SI). However, there was considerable consensus between the types of metabolite identified in separate screens of colon fibroblasts and NHOF-1 oral fibroblasts, where the percentage of SA-βGal-positive cells was 83.1 and 87.9%, respectively (Supplementary Table S3 in the SI), and also when, in a separate screen, the ESMs of all five lines induced to >90% SA-βGal positivity by 20 Gy of γ rays (IrrDSBsen) were compared with their growing controls (Supplementary Table S5 in the SI). To further test the relationship between irreparable DNA DSBs and the ESM, we also compared the NHOF-1 line 5 days after irradiation with repairable (0.5 Gy) or irreparable (20 Gy) levels of DNA damage[16] with unirradiated growing controls (Supplementary Table S5 in the SI). Finally, to test whether the metabolites of the ESM were early or late markers of senescence (or both), we conducted a time course study of NHOF-1 and NHOF-5 oral fibroblasts following 20 Gy of γ rays, and the results are shown in Supplementary Figures S13−S15 in the SI. The relative metabolite abundance data resulting from unbiased global biochemical profiling and their relation-

DOI: 10.1021/pr501221g
J. Proteome Res. 2015, 14, 1854−1871

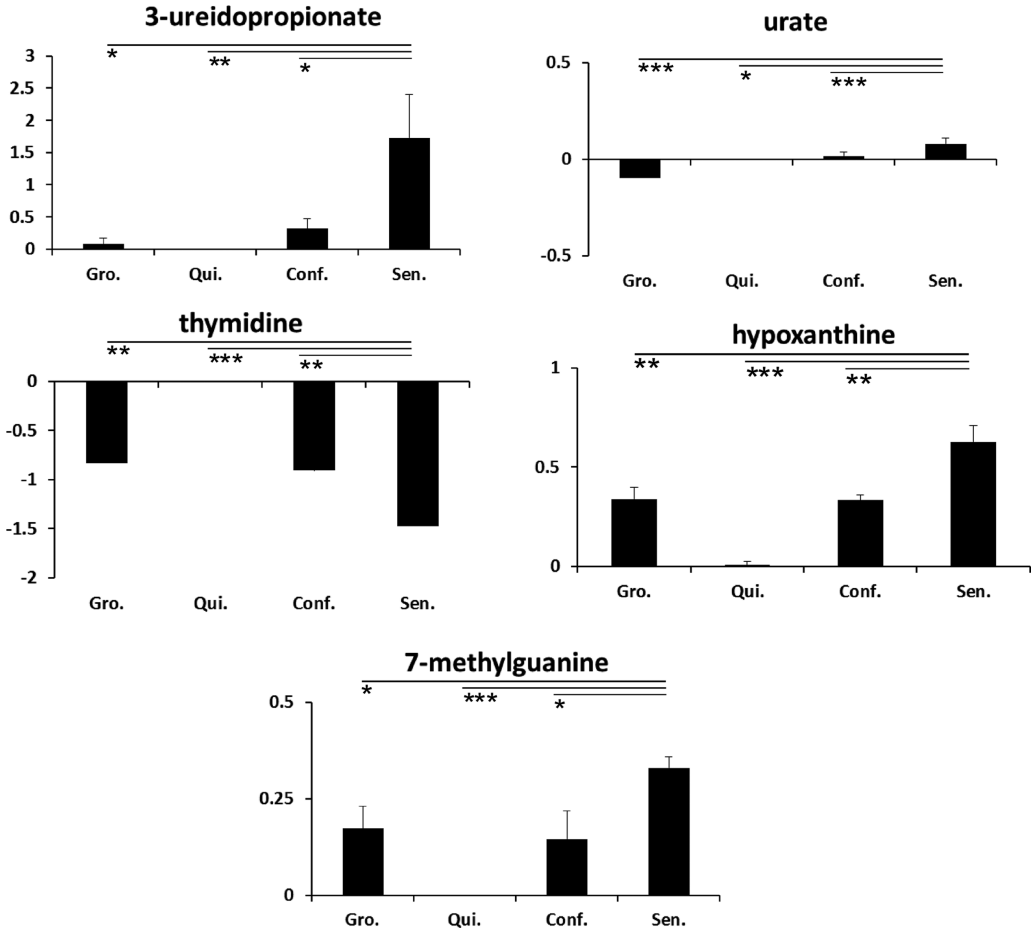

Figure 3. Nucleotide catabolites accumulate and thymidine is depleted in the PEsen ESM relative to growing, quiescent and confluent cells. The Figure shows the net scaled intensity of each metabolite normalized to 1×10^5 cells/mL ± standard deviation in growing, quiescent, confluent, and PEsen NHOF-1 oral fibroblasts. The symbols are the same as for Figure 1. $N = 3$ per cell group.

ship to the pathways discussed later are presented in Figures 1, 3−8, and 10 and Supplementary Figures S1−S6 in the SI. Of more than 3000 known molecules screened, 175−261 molecules were detected in each of the four ESM screens, but not all metabolites were detected in every screen. To determine which metabolic changes were independent of the senescence-associated increase in biomass, we analyzed NHOF-1 cell pellets in parallel with their ESMs and detected 380 metabolites. In the most informative screen, 30/261 metabolites specifically significantly accumulated in senescent cells relative to all control groups, and 13/261 metabolites were depleted (Supplementary Table S3 in the SI). There was some variation between the human cell lines in all four screens, but several metabolites and pathways were consistent in that they were seen in more than one PEsen line (Supplementary Tables S3 and S4 in the SI) or were seen in all five lines tested following IrrDSBsen (Supplementary Table S5 in the SI); these are highlighted later.

Redox Homeostasis

Gamma glutamyl amino acids (GGAAs) play an important role in regulating the exchange of intra- and extracellular glutathione as well as amino acid uptake. Levels of multiple GGAAs, including gamma-glutamylleucine, gamma-glutamylmethionine, gamma-glutamylglutamine, and gamma-glutamylphenylalanine, were elevated in the culture media from PEsen NHOF-1 cells relative to growing, quiescent, and confluent control cells, and the last three were elevated in the ESM of more than one PEsen line where detectable (Supplementary Table S3 in the SI, Figure 1). The catabolic product of GGAAs, 5′-oxoproline, was unchanged in both PEsen and IrrDSBsen cells, but cysteine-glutathione disulfide, which is formed under oxidative stress conditions by the reaction of cysteine with glutathione, was elevated and showed a trend in PEsen colon fibroblasts (Supplementary Table S3 in the SI, Figure 1). Metabolites involved in cysteine metabolism (cysteine sulfonic acid and hypotaurine) were also specifically elevated in PEsen NHOF-1 cells (Supplementary Table S3 in the SI, Figure 1), and cysteine was elevated in PEsen colon fibroblasts (Supplementary Table S3 in the SI). In addition, another metabolite indicative of increased oxidative damage response, the vitamin B6 metabolite, pyridoxate, was also specifically elevated in the ESM of PEsen NHOF-1 cells and also elevated in PEsen colon cells (Supplementary Table S3 in the SI).

To gain some insight into whether the increase in the levels of the above metabolites was the result of an increase in PEsen biomass, we examined the levels of the previously described metabolites in NHOF-1 cell pellets, from which the ESMs in Supplementary Table S3 in the SI were derived. It can be seen from Supplementary Figure S1 in the SI that protein-normalized levels of gamma-glutamylphenylalanine, gamma-glutamylalanine, cysteine sulfonic acid, and hypotaurine were elevated in PEsen NHOF-1 cells relative to the growing, quiescent, and confluent controls. However, other GGAAs,

DOI: 10.1021/pr501221g
J. Proteome Res. 2015, 14, 1854−1871

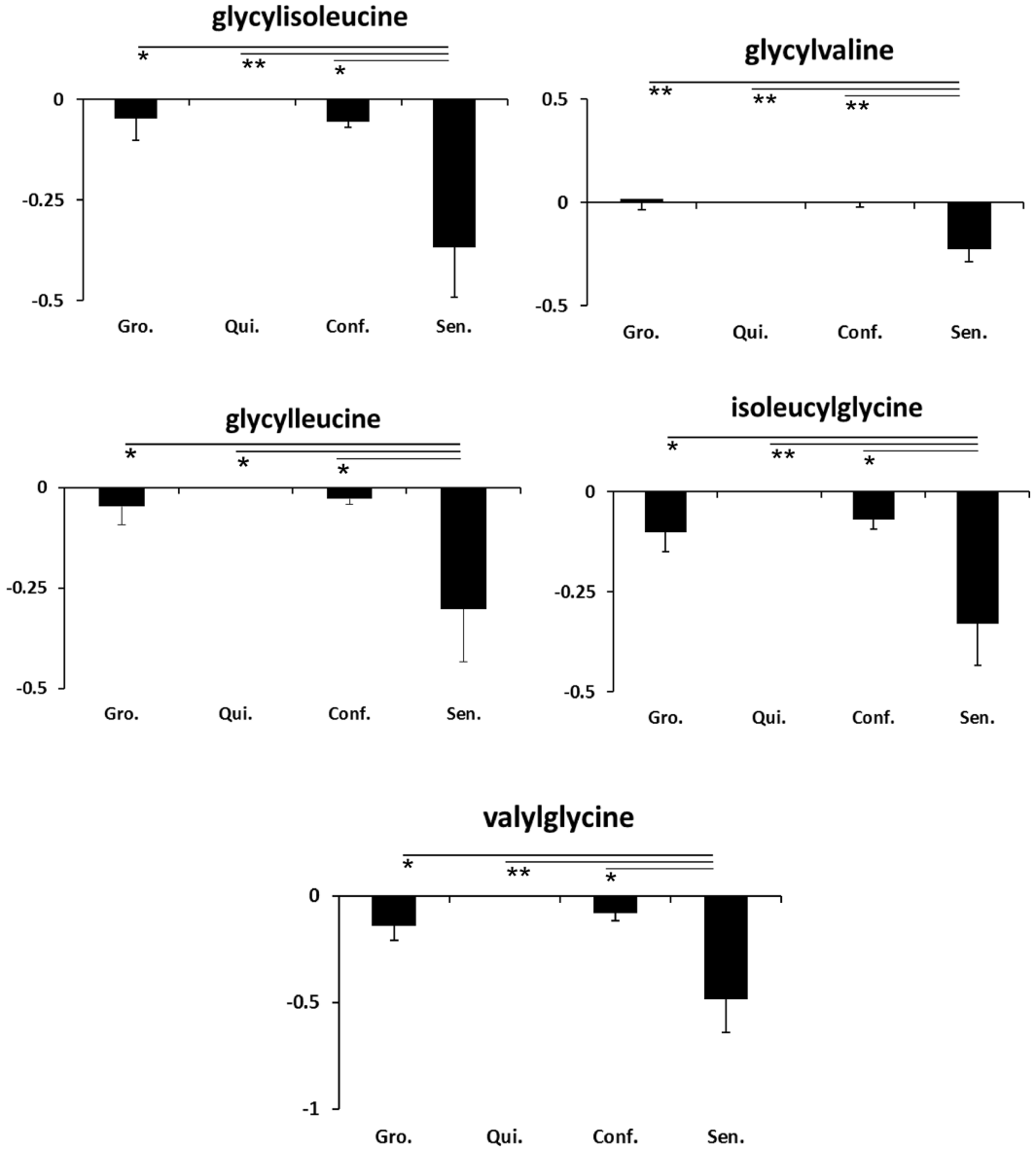

Figure 4. Multiple dipeptides are depleted in the PEsen ESM relative to growing, quiescent, and confluent cells. The Figure shows the net scaled intensity of each metabolite normalized to 1×10^5 cells/mL ± standard deviation in growing, quiescent, confluent, and PEsen NHOF-1 oral fibroblasts. The symbols are the same as for Figure 1. $N = 3$ per cell group.

cysteine, cysteine glutathione disulfide, and reduced glutathione, were unchanged or depleted. Thus, there is no straightforward relationship between the PEsen biomass and the ESM, and further work to examine issues such as alterations in transport or flux will be required to explain these observations.

To further test for the role of oxidative damage in the ESM, we tested for levels of enzyme transcripts involved in this process using qPCR. We show that the oxidative damage enzymes whose transcripts were upregulated by more than 2 fold and were statistically significant in both PEsen and IrrDSBsen encoded secreted, lipid membrane, cytosolic, or glutathione metabolism proteins (Figure 2); these included *NOX5*, *PRNP*, *PTGS2*, and *SFTPD* and additionally a large but nonsignificant up-regulation of *SOD3*. An additional significant greater than 2-fold up-regulation of *DUOX1* and *PTGS1* was noted in IrrDSBsen. A full list of the enzymes tested and their full names is given in Supplementary Table S6 in the SI. The enzyme gamma-glutamyl transferase (GGT) transfers the gamma-glutamyl moiety of glutathione to an amino acid acceptor to provide cysteine for de novo glutathione synthesis. Thus, elevated GGAAs may result from increased GGT activity, glutathione availability, or disruption in redox homeostasis or decreased catabolism. However, the absence of an alteration in the catabolic product 5′-oxoproline and the increase in glutathione disulfide argues in favor of altered redox homeostasis, and several enzyme transcripts involved in oxidative defense were also elevated in both PEsen and IrrDSBsen cells. These data suggest a disruption in redox metabolism and are consistent with reports of increased GGT activity in senescence[26] and may contribute to alterations in dipeptide levels because these can indicate reduced protein catabolism (see later).

Nucleotide Metabolism

There was a depletion of thymidine and an increase in both purine (hypoxanthine, 7-methylguanine, and urate) and

DOI: 10.1021/pr501221g
J. Proteome Res. 2015, 14, 1854−1871

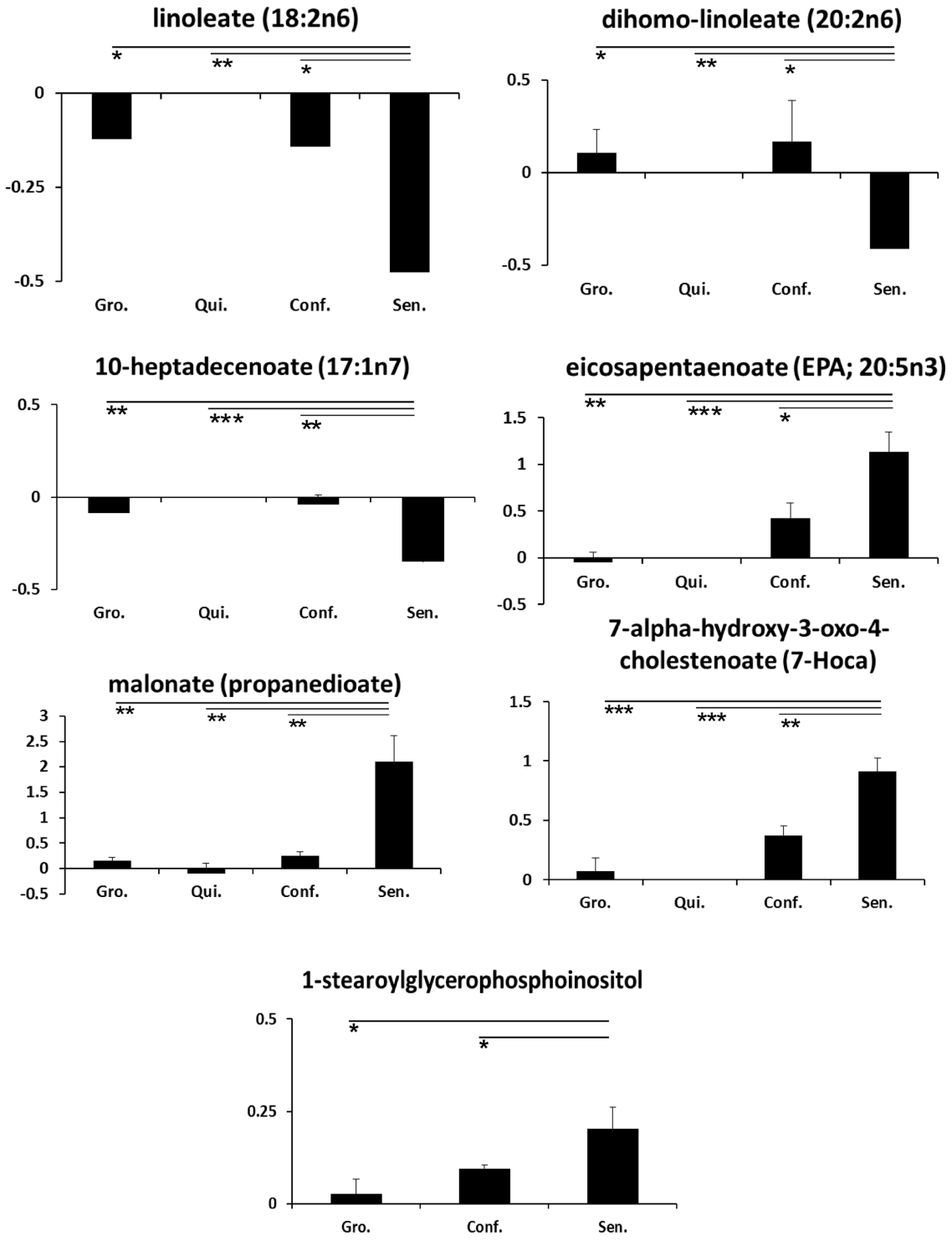

Figure 5. Essential fatty acids and their precursors are modulated in the PEsen ESM relative to growing, quiescent and confluent cells. The Figure shows the net scaled intensity of each metabolite normalized to 1×10^5 cells/mL ± standard deviation in growing, quiescent, confluent, and PEsen NHOF-1 oral fibroblasts. The symbols are the same as for Figure 1. $N = 3$ per cell group.

pyrimidine (3-ureidoproprionate) catabolic products in both PEsen (Supplementary Table S3 in the SI, Figure 3) and IrrDSBsen cells. Furthermore, urate, which is accompanied by the production of hydrogen peroxide, was also elevated in PEsen NHOF-1 relative to the growing, quiescent, and confluent controls (Supplementary Table S3 in the SI and Figure 3), suggesting that the higher levels of nucleotide catabolism may support oxidative stress. Thymidine was not detectably depleted within the NHOF-1 cells relative to the growing, quiescent, and confluent cells when corrected for protein content, but hypoxanthine and 3-ureidoproprionate both accumulated, indicating that the accumulation of both these metabolites is independent of the increased senescent cell biomass (Supplementary Figure S2 in the SI). The depletion of thymidine in the medium of senescent cells suggests increased nucleic acid turnover or altered redox homeostasis in the

DOI: 10.1021/pr501221g
J. Proteome Res. 2015, 14, 1854−1871

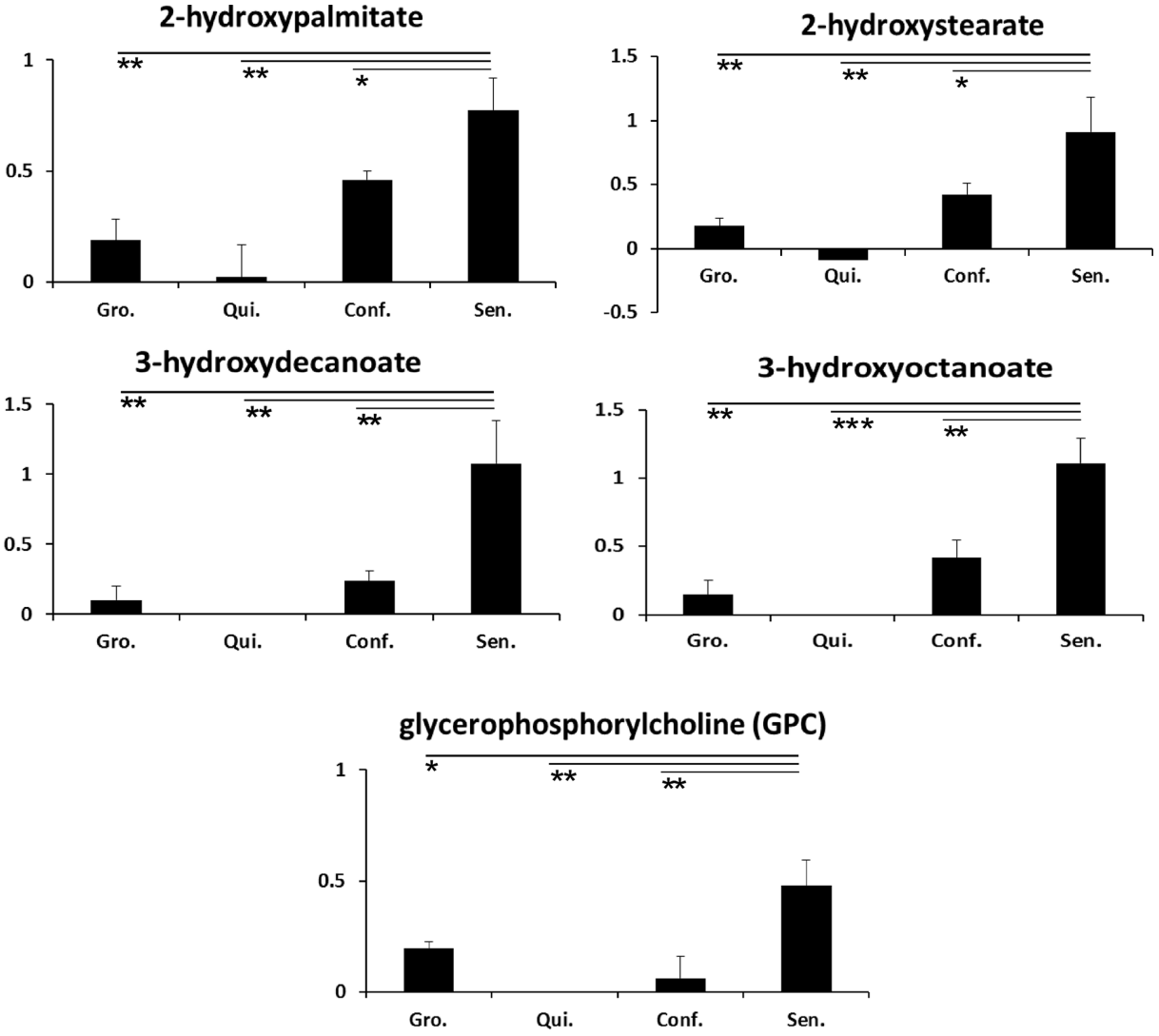

Figure 6. Phospholipid catabolites and monohydroxy fatty acids accumulate in the PEsen ESM relative to growing, quiescent, and confluent cells. The Figure shows the net scaled intensity of each metabolite normalized to 1×10^5 cells/mL ± standard deviation in growing, quiescent, confluent, and PEsen NHOF-1 oral fibroblasts. The symbols are the same as for Figure 1. $N = 3$ per cell group.

senescent cells (see above), as there was an increase in both purine (hypoxanthine and urate) and pyrimidine (3-ureidopropionate) catabolic products.

Dipeptides

Multiple dipeptides were diminished in NHOF-1 PEsen ESM when compared with growing, quiescent, and confluent cells (Supplementary Table S3 in the SI, Figure 4). Glycylisoleucine was also significantly depleted in PEsen colon fibroblasts relative to growing controls (Supplementary Table S3 in the SI), and glycylleucine, glycylvaline, isoleucylglycine, and valylglycine showed a trend for depletion. In addition, glycylvaline was significantly depleted, and valylaspartate showed a strong trend for depletion when all five PEsen lines were compared with their growing controls (Supplementary Table S4 in the SI).

Glycylleucine, glycylvaline, isoleucylglycine, valylglutamine, and valylleucine all showed a strong trend for depletion in PEsen NHOF-1 cell pellets relative to their growing, quiescent, and confluent counterparts even when adjusted for protein content (Supplementary Figure S3 in the SI), suggesting that the depletion of the dipeptides was generally independent of biomass.

Notably the dipeptides previously mentioned are exclusively branch-chain amino-acid-related, which may indicate altered branched chain amino transferase (BCAT) or branched chain keto acid dehydrogenase (BCKD) expression or activity, but this hypothesis requires further investigation. Multiple dipeptides were diminished in the senescent cell ESM, perhaps as a result of increased uptake but also due to increased catabolism to supply carbon skeletons for the tricarboxylic acid (TCA) cycle. Differences in dipeptide levels can also result from alterations in protein processing and both protein synthesis and degradation rates in mammals decline with age[27] and oxidation can induce decreased proteosome activity during human fibroblast senescence.[28]

Essential Fatty Acids and Membrane Lipids

Essential fatty acids are vital precursors for the generation of lipid mediators that contribute to regulating proliferation, inflammation, and extracellular matrix remodelling. They are also important for the large increase in membranous organelles that are important components of the cellular senescent

DOI: 10.1021/pr501221g
J. Proteome Res. 2015, 14, 1854−1871

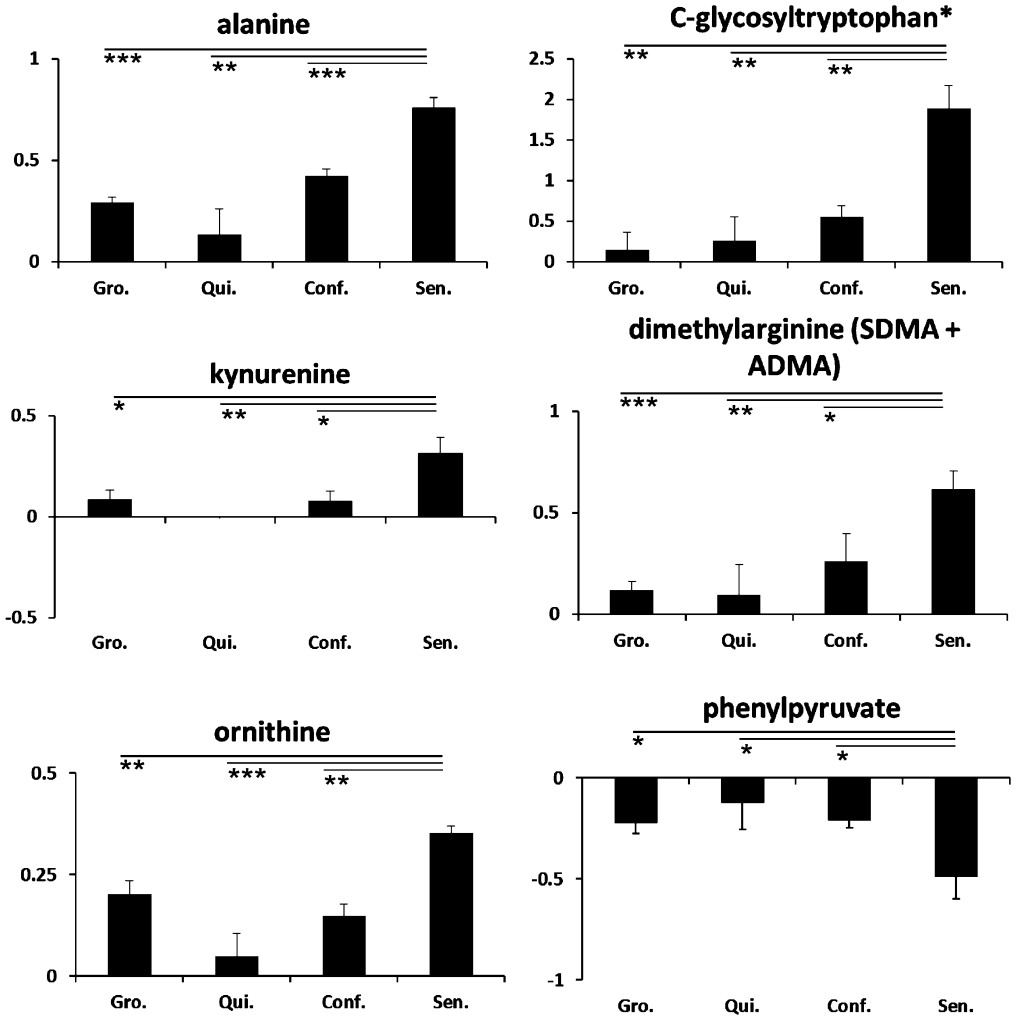

Figure 7. Modulation of amino acid metabolism in the PEsen ESM relative to growing, quiescent and confluent cells. The Figure shows the net scaled intensity of each metabolite normalized to 1×10^5 cells/mL ± standard deviation in growing, quiescent, confluent, and PEsen NHOF-1 oral fibroblasts. The symbols are the same as for Figure 1. $N = 3$ per cell group.

phenotype, and there is evidence that this may be mediated by a sterol regulatory element.[29] Some lipids and their intermediates increased in PEsen NHOF-1 cells when compared with growing, quiescent, and confluent cells (Supplementary Table S3 in the SI, Figure 5) including 1-stearoylglycerophosphoinositol, the sterol 7-alpha-hydroxy-3-oxo-4-cholestenoate (7-Hoca), and eicosapentaenoate (EPA; 20:5n3), whereas others such as 10-heptadecenoate (17:1n7), dihomo-linoleate (20:2n6), and linoleate (18:2n6) were depleted. In addition, an intermediate of fatty acid synthesis (malonate propanedioate) was also elevated consistent with increased fatty acid synthesis required for the increase in senescent cell membranes. 1-Stearoylglycerophosphoinositol also showed a strong trend for accumulation when all five PEsen lines were compared with their growing controls (Supplementary Table S4 in the SI), suggesting that this was a robust general marker of PEsen.

In the case of 1-stearoylglycerophosphoinositol, 7-Hoca, dihomo-linoleate (20:2n6), linoleate (18:2n6), and to some extent heptadecenoate (17:1n7), these changes were reflected in the metabolome of the protein-normalized NHOF-1 cell pellets, suggesting that they were not merely a result of increased PEsen biomass; however, EPA showed only a slight trend to accumulate in the PEsen cells (Supplementary Figure S4 in the SI).

There were also increased levels of phospholipid catabolites such as glycerophosphorylcholine (GPC; Supplementary Table S3 in the SI, Figure 6) when PEsen NHOF-1 cells were compared with growing, quiescent, and confluent cells. Aside from phospholipid metabolism, the monohydroxy fatty acids 2-hydroxystearate, 2-hydroxypalmitate, 3-hydroxydecanoate, and 3-hydroxyoctanoate were elevated in PEsen NHOF-1 cells when compared with the controls (Supplementary Table S3 in the SI, Figure 6), 2-hydroxystearate and 2-hydroxypalmitate were both elevated in colon fibroblasts compared with growing controls (Supplementary Table S3 in the SI), and 2-hydroxystearate was significantly elevated when all five PEsen lines were compared with growing controls (Supplementary Table S4 in the SI).

2-Hydroxystearate and to a lesser extent 2-hydroxypalmitate accumulated intracellularly relative to the controls, indicating that these metabolites were independent of increased senescent cell biomass but GPC did not and in fact was depleted when compared with the confluent and quiescent controls (Supplementary Figure S5 in the SI).

The elevation of essential fatty acids in senescent cell ESM may reflect changes in uptake from the media or processing for

DOI: 10.1021/pr501221g
J. Proteome Res. 2015, 14, 1854−1871

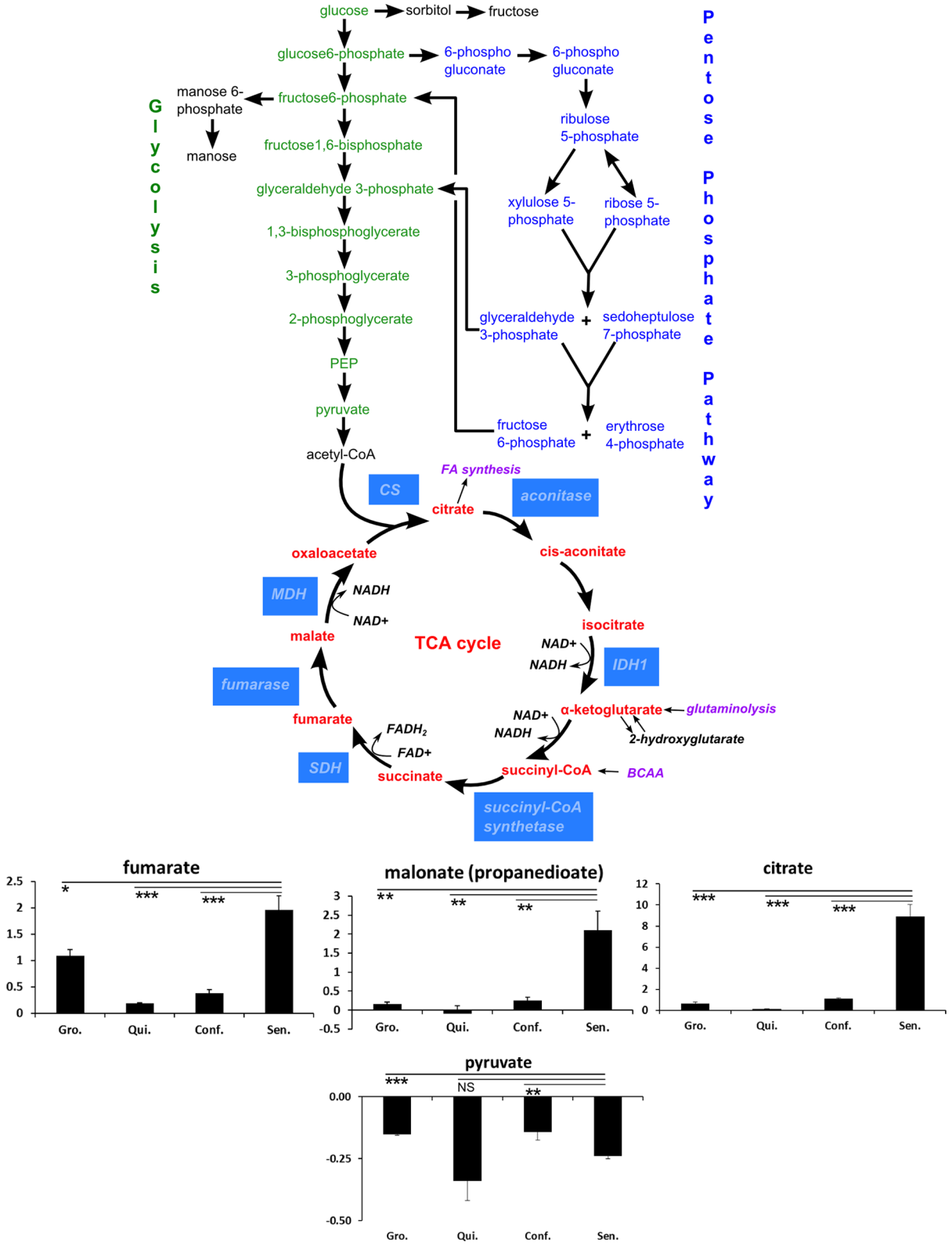

Figure 8. Modulation of energy metabolism in the PEsen ESM relative to growing, quiescent and confluent cells. The Figure shows the pathways involved in energy production and the net scaled intensity of each metabolite normalized to 1×10^5 cells/mL ± standard deviation in growing, quiescent, confluent, and PEsen NHOF-1 oral fibroblasts. The symbols are the same as for Figure 1. $N = 3$ per cell group.

the generation of eicosanoids and may also indicate increased membrane hydrolysis and phospholipase A2 activity. In support of the former hypothesis, prostaglandin E2 has been reported to act on specific receptors to induce both the onset and the maintenance of senescence[30] and accumulates intracellularly in the NHOF-1 PEsen cells relative to the growing and confluent controls. Furthermore, the transcript for the cyclooxygenase 2 gene *PTGS2* is elevated in both PEsen and IrrDBsen. (See

DOI: 10.1021/pr501221g
J. Proteome Res. 2015, 14, 1854−1871

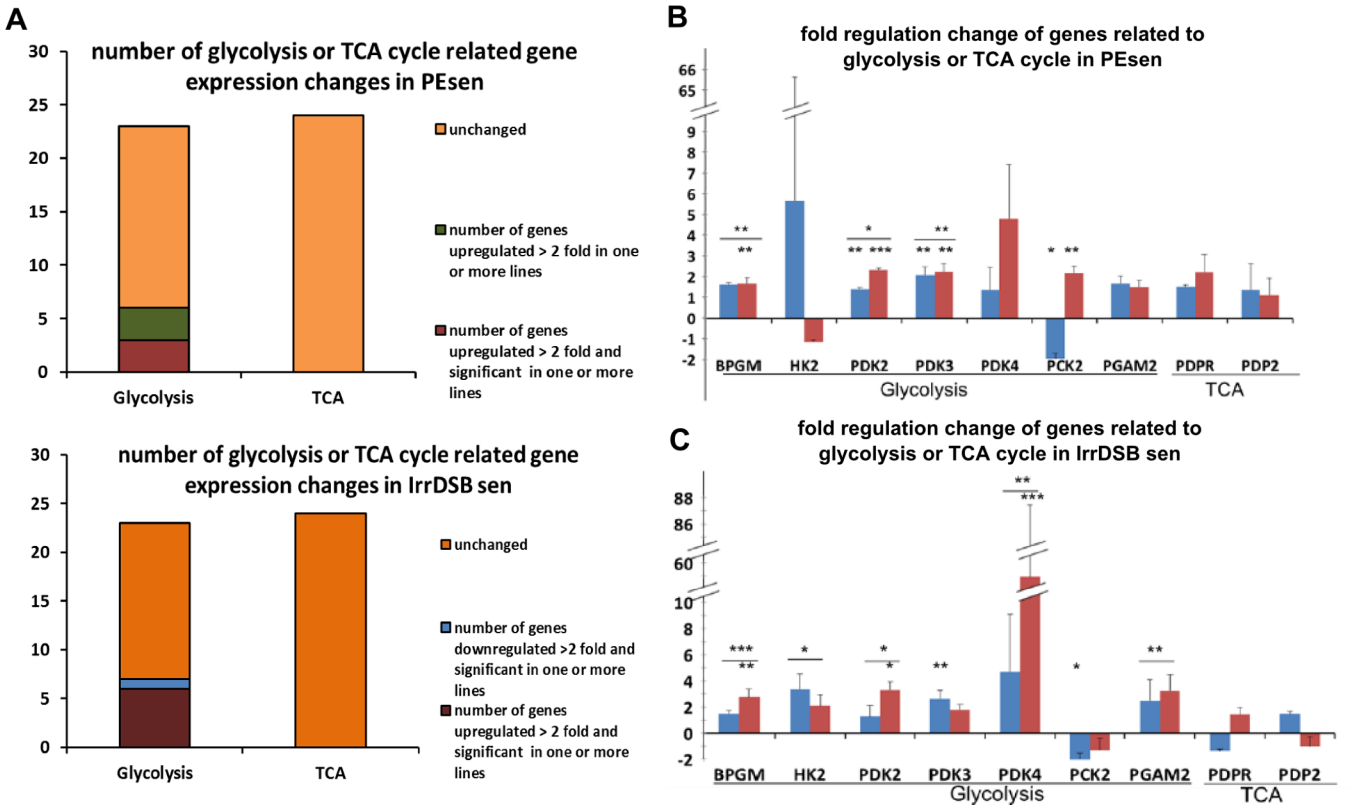

Figure 9. Alterations in glucose metabolism enzymes in PEsen and IrrDSBsen. (A) Number of enzyme genes altered in PEsen (top) and IrrDSBsen (bottom). (B) Data from PEsen. *, $P < 0.05$; **, $P < 0.02$ (Welch's t test). Lines across both bars indicate the level of significance for both cell lines combined. (C) Same data as in panel B but for IrrDSBsen, with the symbols being the same as in panel B. $N = 3$ per cell line in each group.

above and Figure 2.) The latter hypothesis is supported by increased levels of the phospholipid catabolite GPC. Four monohydroxy fatty acids were also elevated, and these molecules are important constituents of sphingolipids that stabilize membrane structure and lipid−protein interactions. Overall, the results are consistent with a disruption of membrane lipids in senescence and a degradation of phospholipids.

Amino Acid Metabolism

Several amino acids alanine, C-glycosyltryptophan and kynurenine (tryptophan metabolism), dimethylarginine (SDMA + ADMA), and ornithine (arginine and proline metabolism) accumulated in the NHOF-1 PEsen ESM when compared with the controls and phenylpyruvate (tyrosine and phenylalanine metabolism) became depleted (Supplementary Table S3 in the SI, Figure 7). The first three metabolites also accumulated in PEsen NHOF-1 cells intracellularly (Supplementary Figure S6 in the SI), suggesting that their accumulation in the ESM was not entirely due to increased senescent cell biomass. Alanine also accumulated significantly when PEsen colon cell ESM was compared with growing controls (Supplementary Table S3 in the SI), and kynurenine showed a weak trend for accumulation. Interestingly, kynurenine is known to suppress T-cell proliferation and NK-cell function[31] and is an intermediate for the generation of the mediators kynurenic acid and quinolinic acid, which can serve as neuronal agonists and antagonists reported to impact Huntington's and Alzheimer's disease.[32] The accumulation of C-glycosyltryptophan is interesting because of its association with chronological age and healthspan traits such as low birth weight[19] (see later) and may be related to a highly significant and specific depletion of several sugar nucleotides in PEsen cells (James et al., manuscript in preparation) that act as donors for some glycosyltransferases and thus may indicate an increase in the activity of these enzymes in senescent cells. However, C-glycosylation is specific for tryptophan, and so the accumulation of C-glycosyltryptophan in the ESM and human aging requires further investigation.

Energy Metabolism

The TCA cycle is the major common pathway for the oxidation of carbohydrates, lipids, and select amino acids. An accumulation of citrate and to a lesser extent fumarate was observed in PEsen compared with growing, quiescent, and confluent controls (Supplementary Table S3 in the SI, Figure 8), and citrate was significantly elevated in PEsen colon cells (Supplementary Table S3 in the SI) and in all five PEsen lines (Supplementary Table S4 in the SI) compared with its growing controls. In addition, pyruvate was depleted in the medium of PEsen NHOF-1 cells compared with growing and confluent controls (Supplementary Table S3 in the SI, Figure 8). Intracellular citrate and fumarate levels declined within the PEsen NHOF-1 cells, and pyruvate levels accumulated only slightly, and so the intracellular levels of these metabolites did not explain their alteration in the ESM (see later).

PEsen and IrrDSBsen Fibroblasts Show Reduced TCA Activity and Shift Energy Production toward Glycolysis, Gluconeogenesis, and the Pentose−Phosphate Pathway

The previously described changes may be consistent with increased glycolysis and TCA cycle activity. However, qPCR analysis of the enzyme transcripts involved in glucose

DOI: 10.1021/pr501221g
J. Proteome Res. 2015, 14, 1854−1871

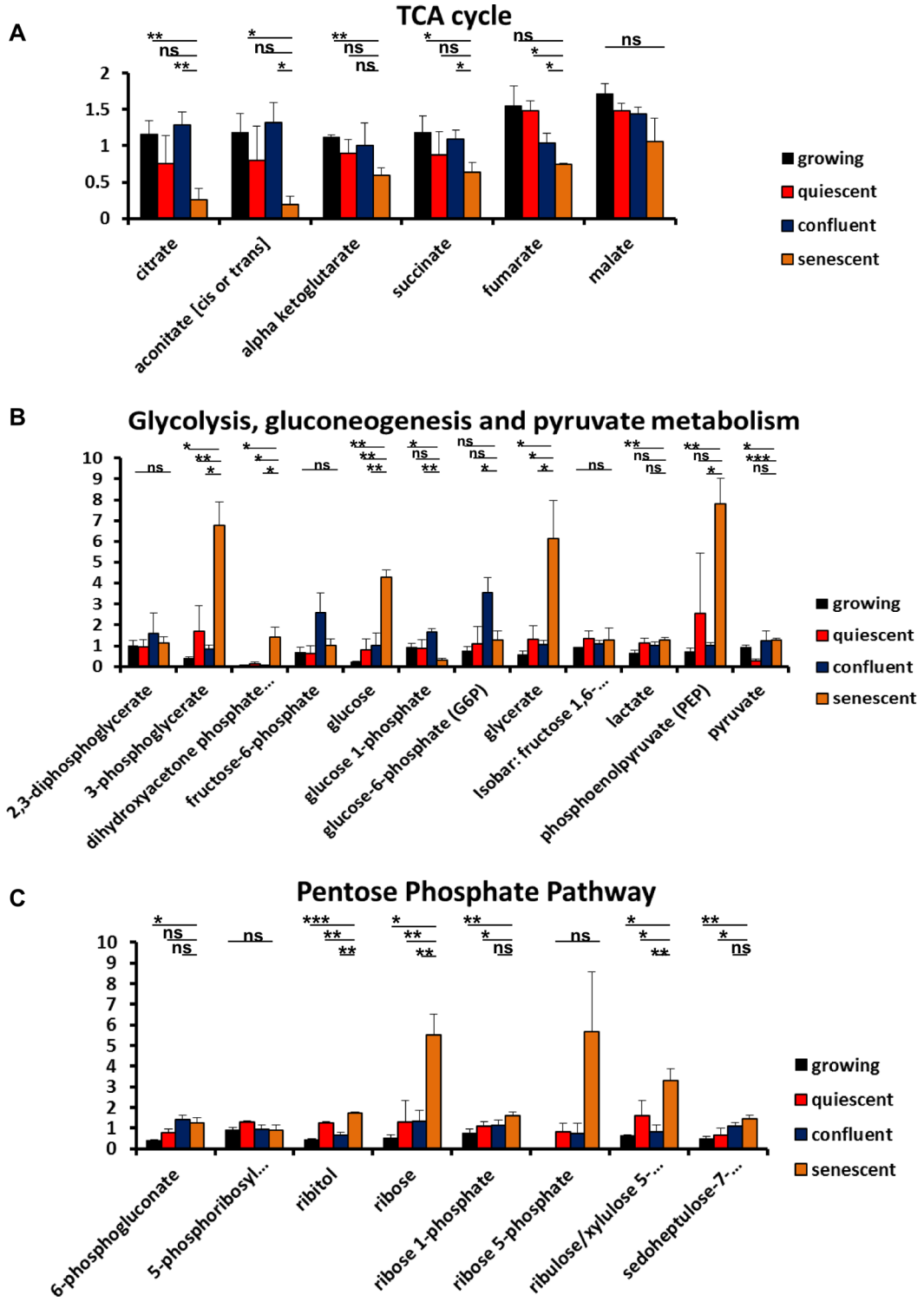

Figure 10. Intracellular levels of energy metabolites in the PEsen cells relative to growing, quiescent, and confluent cells. The Figure shows the scaled intensity of each metabolite normalized to protein ± standard deviation in growing, quiescent, confluent, and PEsen NHOF-1 oral fibroblasts. (A) Metabolites of the TCA cycle. (B) Metabolites of glycolysis and gluconeogenesis. (C) Metabolites of the PPP. The symbols are the same as for Figure 1. $N = 3$ per cell group.

metabolism showed that while many enzymes involved in glycolysis (BPGM, PDK2, PDK3, PDK4) were elevated in both forms of senescence, together with PGAM and HK2 in IrrDSBsen, PCK2 was reduced (Figure 9). The transcription levels of the remaining TCA cycle enzymes examined were normal, and a full list of the enzymes and their full names is given in Supplementary Table S7 in the SI. Examination of the NHOF-1 PEsen intracellular metabolome revealed a reduction in citrate and indeed all TCA metabolites, when normalized for cellular protein, were reduced in PEsen NHOF-1 cells compared with the controls (Figure 10A) and even when normalized for cell number citrate did not show an increase

DOI: 10.1021/pr501221g
J. Proteome Res. 2015, 14, 1854−1871

(data not shown). The decline in protein-normalized citrate levels may be indicative of a decline in mitochondrial metabolism; ultimately, oxidative metabolism was reduced in all three growth-arrested conditions, as evidenced by significantly lower levels of nicotinamide adenine dinucleotide (NADH) compared with growing controls (data not shown). In contrast, high levels of the glycolytic intermediates 3-phosphoglycerate, glucose 6-phosphate, fructose 6-phosphate, and phosphoenolpyruvate in PEsen cells may highlight glycolytic flux to support increased pyruvate and lactate production, and pyruvate was also depleted from the PEsen medium (see above) in both PEsen and IrrDSBsen cells (Figure 10B). In addition, PEsen cells accumulated glucose, and the depletion of glucose-1-phosphate in the same cells (Figure 10B) was consistent with gluconeogenesis and the depletion of glycogen stores. The decrease in intracellular citrate levels is fully consistent with increased glycolysis because high levels of citrate would inhibit glycolysis through phosphofructokinase. Aside from glycolysis, differences in glucose availability may also impact pentose phosphate pathway (PPP) metabolism. In agreement, the PPP metabolites ribose 5-phosphate, ribulose/xylulose 5-phosphate, and sedoheptulose 7-phosphate were elevated in PEsen cells (Figure 10C) compared with their controls and may reflect glucose 6-phosphate shuttling to the PPP to support glutathione detoxification and nicotinamide adenine dinucleotide phosphate (NADPH) regeneration, the latter of which is elevated under all conditions of growth arrest (data not shown).

These results are consistent with compromised mitochondrial function or stalled TCA cycle progression; indeed, mitochondrial dysfunction has been reported in both IrrDSBsen and PEsen.[33] However, increased glycolytic metabolism in senescent cells is surprising because this is a mechanism often used to escape senescence and oxidative stress as, paradoxically, increased glycolysis has been shown to protect cells from senescence.[34] Furthermore, OIS shifts metabolism toward the TCA cycle by regulating the mitochondrial gateway enzyme pyruvate dehydrogenase (PDH) via down-regulation of PDK1 and up-regulation of PDP-2.[17c] Additionally, p53, which is important for the induction and maintenance of senescence,[35] generally suppresses glycolysis and stimulates the TCA cycle while having equivocal effects on the PPP.[36] In the present study, we found that pyruvate dehydrogenase kinase (PDK) 2, 3, and 4 transcripts were elevated, and PDP-2 transcripts showed no change in both PEsen and IrrDSBsen. The difference between our current study in regards to energy metabolism and previous studies on the entry of cells into senescence[17c,34,36,37] was surprising. However, this apparent paradox might be reconciled on the grounds that senescence is a dynamic process; senescence proceeds from a reversible phase involving a high level of p53 activity, exemplified by high levels of $p21^{WAF}$,[9,35,38] which then declines to be supplanted by the accumulation of $p16^{INK4A}$,[9,38] senescence-associated heterochromatic foci,[10] and permanent cell cycle arrest. Indeed, p53 is reported to suppress $p16^{INK4A}$ expression.[39] It was notable that many of the metabolic changes in senescent cells (intracellular and the ESM) were amplified as the senescent phenotype became more advanced and were much more marked in PEsen and IrrDSBsen cultures, where the percentage of senescent cells was >80%. In summary, senescent cells may exhibit increased PPP flux to help restore redox homeostasis while displaying increased glycolytic metabolism in an attempt to avoid further damage and support cell survival, and this may represent a strategy to avoid further damage by diverting energy production away from the TCA cycle. In regards to p53, senescent cells resemble cells with low p53 activity that promotes redox homeostasis (see above) repair and cell survival;[36] this is also consistent with our previous data showing that senescent cells do not have higher levels of 8-hydroxy-2-deoxyguanosine when compared with presenescent cells.[2] In addition, the uric acid transporter SLC2A9 is reported to be a p53 target gene, and uric acid uptake from the serum can reduce ROS levels in cells,[40] and thus the accumulation of urate in the PEsen ESM might be consistent with reduced uptake and thus reduced p53 activity.

The depletion of intracellular citrate could be explained in many ways. First, citrate synthase activity shows reduced activity in PEsen,[41] and cytoplasmic ATP citrate lyase has been reported to be increased in senescent human fibroblasts.[29] ATP citrate lyase is essential for the production of acetyl CoA and fatty acid synthesis required for the large increase in membranous organelles observed in senescent cells. ATP citrate lyase may thus contribute to the depletion of intracellular citrate. Cytoplasmic aconitase is known to be activated by ROS[42] and converts citrate to *cis*-aconitate to generate isocitrate for fatty acid synthesis and other metabolic processes, and intracellular aconitate is also reduced in PEsen NHOF-1 cells.

However, the relative accumulation of citrate in the PEsen and IrrDSBsen ESM is not easily explained by their intracellular metabolomes. Increased citrate efflux or decreased uptake from the serum by the senescent cells are candidate mechanisms for increased citrate in the senescent cell ESM, but further experiments will be needed to address these hypotheses. These include metabolic flux experiments and investigating the citrate transporter proteins such as the plasma membrane isoform of SLC25A1[43] in senescent cells.

Relationship between the PEsen and IrrDSBsen Extracellular Senescence Metabolomes and the Kinetics of the IrrDSBsen Extracellular Senescence Metabolome

When all five lines were induced to undergo IrrDSBsen, several GGAAs, together with cysteine glutathione disulfide, cysteine, and pyridoxate, accumulated relative to growing controls in the ESM after 20 days (Supplementary Table S5 and Supplementary Figure S7 in the SI). Hypoxanthine (Supplementary Figure S8 in the SI), 1-stearoylglycerophosphoinositol, 7-Hoca, GPC, 2-hydroxystearate, 2-hydroxypalmitate (Supplementary Figure S9 in the SI), alanine, aspartate, and citrate (Supplementary Figure S10 in the SI) also accumulated in the IrrDSBsen (Supplementary Table S5 in the SI), and thymidine (Supplementary Figure S8 in the SI) pyruvate (Supplementary Figure S10 in the SI) and also the dipeptides glycylisoleucine, glycylleucine, glycylvaline, leucylglycine, and valylglycine (Supplementary Figure S11 in the SI) became depleted.

To test whether the altered ESM was due to the early establishment of IrrDSBs, we compared the 20 Gy irradiated group, which goes on to senesce after 20 days owing to the development of irreparable DNA DSBs, with cells irradiated with repairable (0.5 Gy) levels of DNA damage as well as growing controls at day 5 after radiation, as described.[16] Gamma-glutamylglutamine, gamma-glutamylleucine, gamma-glutamylphenylalanine, cysteine-glutathione disulfide (Supplementary Figure S12 in the SI), hypoxanthine (Supplementary

DOI: 10.1021/pr501221g
J. Proteome Res. 2015, 14, 1854−1871

Figure S8 in the SI), aspartate, and citrate (Supplementary Figure S10 in the SI) all significantly accumulated, and thymidine (Supplementary Figure S8 in the SI) and pyruvate (Supplementary Figure S10 in the SI) became significantly depleted when cells irradiated with 20 Gy were compared with those irradiated with 0.5 Gy and growing controls at day 5. Alanine (Supplementary Figure S10 in the SI), 7-Hoca (Supplementary Figure S9 in the SI), and cysteine (Supplementary Figure S12 in the SI) also showed a strong trend toward accumulation in the 20 Gy group relative to the controls at day 5; however, 2-hydroxypalmitate, pyridoxate, GPC, and the five dipeptides did not, suggesting that these metabolites accumulated late in the development of the IrrDSBsen ESM.

When senescence is established following the development of IrrDSBs, several proteins of the SASP accumulate with time,[16] and in the present study, we confirmed the accumulation of the SASP protein TIMP-2 in the irradiated NHOF-1- and NHOF-5-conditioned medium.[44] Following γ irradiation, gamma-glutamylglutamine, gamma-glutamylmethionine, gamma-glutamylphenylalanine, cysteine glutathione disulfide, pyridoxal and pyridoxate (Supplementary Figure S13 in the SI), 1-stearoylglycerophosphoinositol, and citrate (Supplementary Figure S14 in the SI) accumulated with time compared with the growing controls, and the difference became increasingly significant. 2-Hydroxystearate and to a lesser extent 2-hydroxypalmitate also accumulated progressively over time in NHOF-1 and NHOF-5 cells following the establishment of IrrDSBsen by 20 Gy of γ irradiation (Supplementary Figure S14 in the SI). Hypoxanthine and alanine also showed a trend for accumulation over time (Supplementary Figure S14 in the SI). Conversely, glycylisoleucine, glycylleucine, glycylvaline, and glycylphenylalanine were progressively depleted with time (Supplementary Figure S15 in the SI). These data show that the senescent PEsen ESM overlaps with IrrDSBsen and that the ESM develops progressively following the establishment of irreparable DSBs analogous to the SASP.[16] ESMs such as alanine, 2-hydroxypalmitate, pyridoxate, and the five dipeptides that are not significantly different in the 20 Gy group from the controls at day 5 become so by day 20, indicating that changes in these metabolites develop at a late stage in the development of the senescent phenotype.

Extracellular Senescence Metabolome and the Aging Metabolome

In this study, we established an ESM of senescent human cells that could find utility in the noninvasive detection of senescent cells that are known to accumulate in a variety of human pathologies, including aging. Regarding energy metabolism, citrate levels have been reported to accumulate with age in rabbits[45] and houseflies.[46] Citrate is reduced in the plasma of long-lived insulin receptor substrate 1 null mouse strain.[18e] We also found the phospholipid catabolite GPC to be elevated in the ESM of PEsen and IrrDSBsen, and consistent with its association with aging in vivo, GPC is reduced in the plasma of the long-lived insulin receptor substrate 1 null mouse strain and long-lived dietary-restricted mice.[18e] Although citrate and GPC are elevated in the long-lived Ames Dwarf mouse,[18e] it has been reported that these mice have increased levels of insulin receptor substrate 1 and insulin signaling,[47] so citrate and GPC appear to correlate with reduced insulin signaling in mouse models of longevity, and this pathway regulates lifespan in a wide range of organisms.[48] Furthermore, insulin signaling[49] and other metabolites or pathways represented in the ESM such as alanine[50] and redox homeostasis[49] have also been reported to be associated with cardiovascular disease, which are a major age-related set of diseases. In addition, increased aspartate, citrate, EPA, urate, and C-glycosyltryptophan were recently reported to be associated with increased age in human twin studies, and these 5 metabolites were part of a 22 metabolite signature that was associated with aging and healthspan parameters, such as birth weight, lung function, bone mineral density, and cholesterol levels;[19] these metabolites also accumulated with age independently of other age-related parameters such as telomere length.[19] Furthermore, because 8 of the 22 metabolites reported in human aging in vivo were not detectable in our study, 5/14 ESM metabolites were also represented in the in vivo aging and healthspan signature, suggesting that cellular senescence may influence the metabolism of aging humans. In all, 17/32 elevated ESM metabolites increase with age in humans, although 3/13 depleted ESM metabolites (pyruvate dihomo-linoleate (20:2n6) and heptadecenoate (17:1n7) also increased with human age.[19] However, it should be acknowledged that we have only examined the ESM of one human cell type senescing predominantly by proliferative exhaustion and the acquisition of IrrDSBs; in vivo the aging metabolome may include contributions from multiple cell types and mechanisms. Finally, urate was also reported to be elevated in mice with telomere dysfunction, and the levels lowered in mice ectopically expressing an epithelium-targeted telomerase catalytic subunit gene, previously shown to increase both lifespan and healthspan.[18d]

ESM and Other Diseases

We observed increased kynurenine levels in the NHOF-1 PEsen ESM compared with controls, and increased levels of neurotoxic kynurenine metabolites in the serum of Alzheimer's disease patients have been reported.[32,51] Furthermore, critical links have been identified between tryptophan metabolism in the blood and neurodegeneration,[52] and both kynurenine and C-glycosyltryptophan were elevated in the PEsen ESM. We observed an accumulation of multiple GGAAs and 7-Hoca in the senescent cell ESM, and elevated serum gamma-glutamyl dipeptides[20a] and 7-Hoca[53] have been reported to be associated with specific human liver diseases, including fibrosis[20a,53] and cancer,[20a] where senescent cells are known to accumulate.[54] Furthermore, senescent cells accumulate in the stroma of many cancer types[4a,55] and oral fibrosis.[2] Alanine, GPC, and hypoxanthine were all elevated in the senescent cell ESM; GPC is elevated in the saliva of oral cancer patients,[20b] and alanine is elevated in the saliva of oral and pancreatic cancer patients[20b] as well as oral dysplasia.[20c] In addition, alanine and hypoxanthine accumulate in the saliva of inflammatory periodontal disease patients,[20b] and senescent cells are induced by inflammation in mouse models.[56] Finally, there is accumulating evidence that normal senescent cells are found in tumor tissue[4a,55] and that glycolytic senescent cells can transfer energy in the form of lactate and ketones to the cancer cells and can promote tumor growth and progression in xenografts.[55a] We found no convincing evidence of the accumulation of lactate or ketones in the ESM but did find strong evidence of the accumulation of citrate. Citrate is normally secreted by the prostate gland into the semen as an energy source for sperm but is not secreted by prostate carcinoma cells.[43b] Interestingly, senescent cells are prominent in benign prostatic hyperplasia,[57] and the addition of citrate to

DOI: 10.1021/pr501221g
J. Proteome Res. 2015, 14, 1854−1871

prostate carcinoma cells enhances their metastatic phenotypes, such as loss of adhesion in vitro.[58] Thus, senescent cell-derived citrate may contribute to tumor development and progression.

CONCLUSIONS

Our results have established extracellular metabolomic profiles of PEsen and IrrDSBs that may provide useful noninvasive biomarkers of human cellular senescence, which accumulate in a variety of human pathologies, including aging, inflammation, fibrosis, and neoplasia. Our results also suggest that the accumulation of senescent cells may make a bigger contribution to human pathologies than previously realized and the characterization of the senescent cell ESM may also aid our understanding of the network of metabolic changes that accompany the senescent phenotype. The data also support the hypothesis that the deletion of senescent cells, if achievable in humans, may have a widespread effect on health.

ASSOCIATED CONTENT

Supporting Information

Experimental procedures. Table S1. Characterization of growing, quiescent, confluent, and PEsen cells. Table S2. Characterization of NHOF-1 cells in Table S3 (for 1-stearoylglycerophosphoinositol only). Table S3. Senescence-specific ESMs identified in NHOF-1 and colon fibroblasts. Table S4. Subset of ESMs are consistent markers of PEsen. Table S5. Subset of the ESM is induced by IrrDSBsen. Table S6. Oxidative damage genes analyzed by qPCR. Table S7. Glucose metabolism genes analyzed by qPCR. Figure S1. Modulation of intracellular redox metabolites in PEsen NHOF-1 cells relative to growing, quiescent, and confluent cells. Figure S2. Modulation of intracellular nucleotide catabolites in PEsen NHOF-1 cells relative to growing, quiescent and confluent cells. Figure S3. Multiple intracellular dipeptides are depleted in PEsen NHOF-1 cells relative to growing, quiescent, and confluent cells. Figure S4. Intracellular essential fatty acids and their precursors are modulated in PEsen NHOF-1 cells relative to growing, quiescent and confluent cells. Figure S5. Intracellular phospholipid catabolites and monohydroxy fatty acids accumulate in PEsen NHOF-1 cells relative to growing, quiescent and confluent cells. Figure S6. Modulation of amino acid intracellular metabolism in PEsen NHOF-1 cells relative to growing, quiescent, and confluent cells. Figure S7. Glutathione metabolites accumulate in the ESM following the induction of IrrDSBs. Figure S8. Nucleotide catabolites are modulated in the ESM following the induction of IrrDSBs. Figure S9. Various lipids and phospholipids catabolites accumulate in the ESM following the induction of IrrDSBs. Figure S10. Citrate, alanine, and aspartate accumulate in the ESM following the induction of IrrDSBs. Figure S11. Multiple dipeptides become depleted in the ESM following the induction of IrrDSBs. Figure S12. Glutathione metabolites accumulate early in the ESM following the induction of IrrDSBs and are associated with irreparable as opposed to repairable DNA damage. Figure S13. Glutathione metabolites progressively accumulate in the ESM following the induction of IrrDSBs. Figure S14. Multiple metabolites are progressively modulated in the ESM following the induction of IrrDSBs. Figure S15. Multiple dipeptides are progressively depleted in the ESM following the induction of IrrDSBs. Supplementary Reference. This material is available free of charge via the Internet at http://pubs.acs.org.

AUTHOR INFORMATION

Corresponding Author

*Phone: 44-(0)207-882-7185. Fax: 44(0)207-882-7137. E-mail: e.k.parkinson@qmul.ac.uk.

Present Address

[§]E.K.P.: Centre for Clinical & Diagnostic Oral Sciences, Blizard Institute, 4 Newark Street, London E1 2AT, U.K.

Notes

The authors declare no competing financial interest.

ACKNOWLEDGMENTS

We thank Cleo Bishop, James Koh, and Chris Paraskeva for their generous gifts of the $p16^{INK4A}$ antibody (C.B. and J.K.) and colon fibroblasts (C.P.). We are grateful to Kenny Linton and the Blizard Institute Molecular and Cellular Biology of Medicine Theme for financial support. E.J. is in receipt of the James Paget Ph.D. studentship, and A.D.C. was supported by a Research into Ageing (Age U.K.) Ph.D. studentship.

REFERENCES

(1) (a) Dimri, G. P.; Lee, X.; Basile, G.; Acosta, M.; Scott, G.; Roskelley, C.; Medrano, E. E.; Linskens, M.; Rubelj, I.; Pereira-Smith, O.; et al. A biomarker that identifies senescent human cells in culture and in aging skin in vivo. *Proc. Natl. Acad. Sci. U. S. A.* **1995**, *92* (20), 9363−9367. (b) Herbig, U.; Ferreira, M.; Condel, L.; Carey, D.; Sedivy, J. M. Cellular senescence in aging primates. *Science* **2006**, *311* (5765), 1257. (c) Jeyapalan, J. C.; Ferreira, M.; Sedivy, J. M.; Herbig, U. Accumulation of senescent cells in mitotic tissue of aging primates. *Mech. Ageing Dev.* **2007**, *128* (1), 36−44.

(2) Pitiyage, G. N.; Slijepcevic, P.; Gabrani, A.; Chianea, Y. G.; Lim, K. P.; Prime, S. S.; Tilakaratne, W. M.; Fortune, F.; Parkinson, E. K. Senescent mesenchymal cells accumulate in human fibrosis by a telomere-independent mechanism and ameliorate fibrosis through matrix metalloproteinases. *J. Pathol.* **2011**, *223* (5), 604−617.

(3) Mendez, M. V.; Stanley, A.; Park, H. Y.; Shon, K.; Phillips, T.; Menzoian, J. O. Fibroblasts cultured from venous ulcers display cellular characteristics of senescence. *J. Vasc. Surg.* **1998**, *28* (5), 876−883.

(4) (a) Yang, G.; Rosen, D. G.; Zhang, Z.; Bast, R. C., Jr.; Mills, G. B.; Colacino, J. A.; Mercado-Uribe, I.; Liu, J. The chemokine growth-regulated oncogene 1 (Gro-1) links RAS signaling to the senescence of stromal fibroblasts and ovarian tumorigenesis. *Proc. Natl. Acad. Sci. U. S. A.* **2006**, *103* (44), 16472−16477. (b) Bartkova, J.; Rezaei, N.; Liontos, M.; Karakaidos, P.; Kletsas, D.; Issaeva, N.; Vassiliou, L. V.; Kolettas, E.; Niforou, K.; Zoumpourlis, V. C.; Takaoka, M.; Nakagawa, H.; Tort, F.; Fugger, K.; Johansson, F.; Sehested, M.; Andersen, C. L.; Dyrskjot, L.; Orntoft, T.; Lukas, J.; Kittas, C.; Helleday, T.; Halazonetis, T. D.; Bartek, J.; Gorgoulis, V. G. Oncogene-induced senescence is part of the tumorigenesis barrier imposed by DNA damage checkpoints. *Nature* **2006**, *444* (7119), 633−637.

(5) (a) Xue, W.; Zender, L.; Miething, C.; Dickins, R. A.; Hernando, E.; Krizhanovsky, V.; Cordon-Cardo, C.; Lowe, S. W. Senescence and tumour clearance is triggered by p53 restoration in murine liver carcinomas. *Nature* **2007**, *445* (7128), 656−660. (b) Tomas-Loba, A.; Flores, I.; Fernandez-Marcos, P. J.; Cayuela, M. L.; Maraver, A.; Tejera, A.; Borras, C.; Matheu, A.; Klatt, P.; Flores, J. M.; Vina, J.; Serrano, M.; Blasco, M. A. Telomerase reverse transcriptase delays aging in cancer-resistant mice. *Cell* **2008**, *135* (4), 609−622. (c) Krizhanovsky, V.; Yon, M.; Dickins, R. A.; Hearn, S.; Simon, J.; Miething, C.; Yee, H.; Zender, L.; Lowe, S. W. Senescence of activated stellate cells limits liver fibrosis. *Cell* **2008**, *134* (4), 657−667. (d) Kang, T. W.; Yevsa, T.; Woller, N.; Hoenicke, L.; Wuestefeld, T.; Dauch, D.; Hohmeyer, A.; Gereke, M.; Rudalska, R.; Potapova, A.; Iken, M.; Vucur, M.; Weiss, S.; Heikenwalder, M.; Khan, S.; Gil, J.; Bruder, D.; Manns, M.; Schirmacher, P.; Tacke, F.; Ott, M.; Luedde, T.; Longerich, T.;

DOI: 10.1021/pr501221g
J. Proteome Res. 2015, 14, 1854−1871

Kubicka, S.; Zender, L. Senescence surveillance of pre-malignant hepatocytes limits liver cancer development. *Nature* **2011**, *479* (7374), 547−551. (e) Jun, J. I.; Lau, L. F. The matricellular protein CCN1 induces fibroblast senescence and restricts fibrosis in cutaneous wound healing. *Nat. Cell Biol.* **2010**, *12* (7), 676−685. (f) Baker, D. J.; Wijshake, T.; Tchkonia, T.; LeBrasseur, N. K.; Childs, B. G.; van de Sluis, B.; Kirkland, J. L.; van Deursen, J. M. Clearance of p16Ink4a-positive senescent cells delays ageing-associated disorders. *Nature* **2011**, *479* (7372), 232−236.

(6) Funayama, R.; Ishikawa, F. Cellular senescence and chromatin structure. *Chromosoma* **2007**, *116* (5), 431−440.

(7) (a) d'Adda di Fagagna, F.; Reaper, P. M.; Clay-Farrace, L.; Fiegler, H.; Carr, P.; Von Zglinicki, T.; Saretzki, G.; Carter, N. P.; Jackson, S. P. A DNA damage checkpoint response in telomere-initiated senescence. *Nature* **2003**, *426* (6963), 194−198. (b) Takai, H.; Smogorzewska, A.; de Lange, T. DNA damage foci at dysfunctional telomeres. *Curr. Biol.* **2003**, *13* (17), 1549−1556.

(8) Di Micco, R.; Fumagalli, M.; Cicalese, A.; Piccinin, S.; Gasparini, P.; Luise, C.; Schurra, C.; Garre, M.; Nuciforo, P. G.; Bensimon, A.; Maestro, R.; Pelicci, P. G.; d'Adda di Fagagna, F. Oncogene-induced senescence is a DNA damage response triggered by DNA hyper-replication. *Nature* **2006**, *444* (7119), 638−642.

(9) Alcorta, D. A.; Xiong, Y.; Phelps, D.; Hannon, G.; Beach, D.; Barrett, J. C. Involvement of the cyclin-dependent kinase inhibitor p16 (INK4a) in replicative senescence of normal human fibroblasts. *Proc. Natl. Acad. Sci. U. S. A.* **1996**, *93* (24), 13742−13747.

(10) Narita, M.; Nunez, S.; Heard, E.; Lin, A. W.; Hearn, S. A.; Spector, D. L.; Hannon, G. J.; Lowe, S. W. Rb-mediated heterochromatin formation and silencing of E2F target genes during cellular senescence. *Cell* **2003**, *113* (6), 703−716.

(11) (a) Fumagalli, M.; Rossiello, F.; Clerici, M.; Barozzi, S.; Cittaro, D.; Kaplunov, J. M.; Bucci, G.; Dobreva, M.; Matti, V.; Beausejour, C. M.; Herbig, U.; Longhese, M. P.; d'Adda di Fagagna, F.; Telomeric, D. N. A. damage is irreparable and causes persistent DNA-damage-response activation. *Nat. Cell Biol.* **2012**, *14* (4), 355−365. (b) Hewitt, G.; Jurk, D.; Marques, F. D.; Correia-Melo, C.; Hardy, T.; Gackowska, A.; Anderson, R.; Taschuk, M.; Mann, J.; Passos, J. F. Telomeres are favoured targets of a persistent DNA damage response in ageing and stress-induced senescence. *Nat. Commun.* **2012**, *3*, 708.

(12) Hubackova, S.; Krejcikova, K.; Bartek, J.; Hodny, Z. IL1- and TGFbeta-Nox4 signaling, oxidative stress and DNA damage response are shared features of replicative, oncogene-induced, and drug-induced paracrine 'bystander senescence'. *Aging (N. Y.)* **2012**, *4* (12), 932−951.

(13) Acosta, J. C.; Banito, A.; Wuestefeld, T.; Georgilis, A.; Janich, P.; Morton, J. P.; Athineos, D.; Kang, T. W.; Lasitschka, F.; Andrulis, M.; Pascual, G.; Morris, K. J.; Khan, S.; Jin, H.; Dharmalingam, G.; Snijders, A. P.; Carroll, T.; Capper, D.; Pritchard, C.; Inman, G. J.; Longerich, T.; Sansom, O. J.; Benitah, S. A.; Zender, L.; Gil, J. A complex secretory program orchestrated by the inflammasome controls paracrine senescence. *Nat. Cell Biol.* **2013**, *15* (8), 978−990.

(14) Coppe, J. P.; Patil, C. K.; Rodier, F.; Sun, Y.; Munoz, D. P.; Goldstein, J.; Nelson, P. S.; Desprez, P. Y.; Campisi, J. Senescence-associated secretory phenotypes reveal cell-nonautonomous functions of oncogenic RAS and the p53 tumor suppressor. *PLoS Biol.* **2008**, *6* (12), 2853−2868.

(15) Jiang, H.; Schiffer, E.; Song, Z.; Wang, J.; Zurbig, P.; Thedieck, K.; Moes, S.; Bantel, H.; Saal, N.; Jantos, J.; Brecht, M.; Jeno, P.; Hall, M. N.; Hager, K.; Manns, M. P.; Hecker, H.; Ganser, A.; Dohner, K.; Bartke, A.; Meissner, C.; Mischak, H.; Ju, Z.; Rudolph, K. L. Proteins induced by telomere dysfunction and DNA damage represent biomarkers of human aging and disease. *Proc. Natl. Acad. Sci. U. S. A.* **2008**, *105* (32), 11299−11304.

(16) Rodier, F.; Coppe, J. P.; Patil, C. K.; Hoeijmakers, W. A.; Munoz, D. P.; Raza, S. R.; Freund, A.; Campeau, E.; Davalos, A. R.; Campisi, J. Persistent DNA damage signalling triggers senescence-associated inflammatory cytokine secretion. *Nat. Cell Biol.* **2009**, *11* (8), 973−979.

(17) (a) Aird, K. M.; Zhang, G.; Li, H.; Tu, Z.; Bitler, B. G.; Garipov, A.; Wu, H.; Wei, Z.; Wagner, S. N.; Herlyn, M.; Zhang, R. Suppression of nucleotide metabolism underlies the establishment and maintenance of oncogene-induced senescence. *Cell Rep.* **2013**, *3* (4), 1252−1265. (b) Jiang, P.; Du, W.; Mancuso, A.; Wellen, K. E.; Yang, X. Reciprocal regulation of p53 and malic enzymes modulates metabolism and senescence. *Nature* **2013**, *493* (7434), 689−693. (c) Kaplon, J.; Zheng, L.; Meissl, K.; Chaneton, B.; Selivanov, V. A.; Mackay, G.; van der Burg, S. H.; Verdegaal, E. M.; Cascante, M.; Shlomi, T.; Gottlieb, E.; Peeper, D. S. A key role for mitochondrial gatekeeper pyruvate dehydrogenase in oncogene-induced senescence. *Nature* **2013**, *498* (7452), 109−112. (d) Quijano, C.; Cao, L.; Fergusson, M. M.; Romero, H.; Liu, J.; Gutkind, S.; Rovira, I. I.; Mohney, R. P.; Karoly, E. D.; Finkel, T. Oncogene-induced senescence results in marked metabolic and bioenergetic alterations. *Cell Cycle* **2012**, *11* (7), 1383−1392.

(18) (a) Fuchs, S.; Bundy, J. G.; Davies, S. K.; Viney, J. M.; Swire, J. S.; Leroi, A. M. A metabolic signature of long life in Caenorhabditis elegans. *BMC Biol.* **2010**, *8*, 14. (b) Houtkooper, R. H.; Argmann, C.; Houten, S. M.; Canto, C.; Jeninga, E. H.; Andreux, P. A.; Thomas, C.; Doenlen, R.; Schoonjans, K.; Auwerx, J. The metabolic footprint of aging in mice. *Sci. Rep* **2011**, *1*, 134. (c) Martin, F. P.; Spanier, B.; Collino, S.; Montoliu, I.; Kolmeder, C.; Giesbertz, P.; Affolter, M.; Kussmann, M.; Daniel, H.; Kochhar, S.; Rezzi, S. Metabotyping of Caenorhabditis elegans and their culture media revealed unique metabolic phenotypes associated to amino acid deficiency and insulin-like signaling. *J. Proteome Res.* **2011**, *10* (3), 990−1003. (d) Tomas-Loba, A.; Bernardes de Jesus, B.; Mato, J. M.; Blasco, M. A. A metabolic signature predicts biological age in mice. *Aging Cell* **2013**, *12* (1), 93−101. (e) Wijeyesekera, A.; Selman, C.; Barton, R. H.; Holmes, E.; Nicholson, J. K.; Withers, D. J. Metabotyping of long-lived mice using 1H NMR spectroscopy. *J. Proteome Res.* **2012**, *11* (4), 2224−2235.

(19) Menni, C.; Kastenmuller, G.; Petersen, A. K.; Bell, J. T.; Psatha, M.; Tsai, P. C.; Gieger, C.; Schulz, H.; Erte, I.; John, S.; Brosnan, M. J.; Wilson, S. G.; Tsaprouni, L.; Lim, E. M.; Stuckey, B.; Deloukas, P.; Mohney, R.; Suhre, K.; Spector, T. D.; Valdes, A. M. Metabolomic markers reveal novel pathways of ageing and early development in human populations. *Int. J. Epidemiol.* **2013**, *42* (4), 1111−1119.

(20) (a) Soga, T.; Sugimoto, M.; Honma, M.; Mori, M.; Igarashi, K.; Kashikura, K.; Ikeda, S.; Hirayama, A.; Yamamoto, T.; Yoshida, H.; Otsuka, M.; Tsuji, S.; Yatomi, Y.; Sakuragawa, T.; Watanabe, H.; Nihei, K.; Saito, T.; Kawata, S.; Suzuki, H.; Tomita, M.; Suematsu, M. Serum metabolomics reveals gamma-glutamyl dipeptides as biomarkers for discrimination among different forms of liver disease. *J. Hepatol.* **2011**, *55* (4), 896−905. (b) Sugimoto, M.; Wong, D. T.; Hirayama, A.; Soga, T.; Tomita, M. Capillary electrophoresis mass spectrometry-based saliva metabolomics identified oral, breast and pancreatic cancer-specific profiles. *Metabolomics* **2010**, *6* (1), 78−95. (c) Wei, J.; Xie, G.; Zhou, Z.; Shi, P.; Qiu, Y.; Zheng, X.; Chen, T.; Su, M.; Zhao, A.; Jia, W. Salivary metabolite signatures of oral cancer and leukoplakia. *Int. J. Cancer* **2011**, *129* (9), 2207−2217.

(21) Munro, J.; Steeghs, K.; Morrison, V.; Ireland, H.; Parkinson, E. K. Human fibroblast replicative senescence can occur in the absence of extensive cell division and short telomeres. *Oncogene* **2001**, *20* (27), 3541−3552.

(22) Reitman, Z. J.; Jin, G.; Karoly, E. D.; Spasojevic, I.; Yang, J.; Kinzler, K. W.; He, Y.; Bigner, D. D.; Vogelstein, B.; Yan, H. Profiling the effects of isocitrate dehydrogenase 1 and 2 mutations on the cellular metabolome. *Proc. Natl. Acad. Sci. U. S. A.* **2011**, *108* (8), 3270−3275.

(23) Hu, W.; Zhang, C.; Wu, R.; Sun, Y.; Levine, A.; Feng, Z. Glutaminase 2, a novel p53 target gene regulating energy metabolism and antioxidant function. *Proc. Natl. Acad. Sci. U. S. A.* **2010**, *107* (16), 7455−7460.

(24) Dehaven, C. D.; Evans, A. M.; Dai, H.; Lawton, K. A. Organization of GC/MS and LC/MS metabolomics data into chemical libraries. *J. Cheminf.* **2010**, *2* (1), 9.

(25) Evans, A. M.; DeHaven, C. D.; Barrett, T.; Mitchell, M.; Milgram, E. Integrated, nontargeted ultrahigh performance liquid chromatography/electrospray ionization tandem mass spectrometry

DOI: 10.1021/pr501221g
J. Proteome Res. 2015, 14, 1854−1871

platform for the identification and relative quantification of the small-molecule complement of biological systems. *Anal. Chem.* **2009**, *81* (16), 6656−6667.
(26) Takahashi, S.; Seifter, S.; Davidson, A. Enzymes of the gamma-glutamyl cycle in 'aging' WI-38 fibroblasts and in HeLa S3 cells. *Biochim. Biophys. Acta* **1978**, *522* (1), 63−73.
(27) Makrides, S. C. Protein synthesis and degradation during aging and senescence. *Biol. Rev. Cambridge Philos. Soc.* **1983**, *58* (3), 343−422.
(28) Sitte, N.; Merker, K.; Von Zglinicki, T.; Grune, T.; Davies, K. J. Protein oxidation and degradation during cellular senescence of human BJ. fibroblasts: part I–effects of proliferative senescence. *FASEB J.* **2000**, *14* (15), 2495−2502.
(29) Kim, Y. M.; Shin, H. T.; Seo, Y. H.; Byun, H. O.; Yoon, S. H.; Lee, I. K.; Hyun, D. H.; Chung, H. Y.; Yoon, G. Sterol regulatory element-binding protein (SREBP)-1-mediated lipogenesis is involved in cell senescence. *J. Biol. Chem.* **2010**, *285* (38), 29069−29077.
(30) Martien, S.; Pluquet, O.; Vercamer, C.; Malaquin, N.; Martin, N.; Gosselin, K.; Pourtier, A.; Abbadie, C. Cellular senescence involves an intracrine prostaglandin E2 pathway in human fibroblasts. *Biochim. Biophys. Acta* **2013**, *1831* (7), 1217−1227.
(31) Frumento, G.; Rotondo, R.; Tonetti, M.; Damonte, G.; Benatti, U.; Ferrara, G. B. Tryptophan-derived catabolites are responsible for inhibition of T and natural killer cell proliferation induced by indoleamine 2,3-dioxygenase. *J. Exp. Med.* **2002**, *196* (4), 459−468.
(32) Tan, L.; Yu, J. T. The kynurenine pathway in neurodegenerative diseases: mechanistic and therapeutic considerations. *J. Neurol. Sci.* **2012**, *323* (1−2), 1−8.
(33) (a) Dalle Pezze, P.; Nelson, G.; Otten, E. G.; Korolchuk, V. I.; Kirkwood, T. B.; von Zglinicki, T.; Shanley, D. P. Dynamic modelling of pathways to cellular senescence reveals strategies for targeted interventions. *PLoS Comput. Biol.* **2014**, *10* (8), e1003728. (b) Passos, J. F.; Saretzki, G.; Ahmed, S.; Nelson, G.; Richter, T.; Peters, H.; Wappler, I.; Birket, M. J.; Harold, G.; Schaeuble, K.; Birch-Machin, M. A.; Kirkwood, T. B.; von Zglinicki, T. Mitochondrial dysfunction accounts for the stochastic heterogeneity in telomere-dependent senescence. *PLoS Biol.* **2007**, *5* (5), e110.
(34) Kondoh, H.; Lleonart, M. E.; Gil, J.; Wang, J.; Degan, P.; Peters, G.; Martinez, D.; Carnero, A.; Beach, D. Glycolytic enzymes can modulate cellular life span. *Cancer Res.* **2005**, *65* (1), 177−185.
(35) Beausejour, C. M.; Krtolica, A.; Galimi, F.; Narita, M.; Lowe, S. W.; Yaswen, P.; Campisi, J. Reversal of human cellular senescence: roles of the p53 and p16 pathways. *EMBO J.* **2003**, *22* (16), 4212−4222.
(36) Gottlieb, E.; Vousden, K. H. p53 regulation of metabolic pathways. *Cold Spring Harb Perspect. Biol.* **2010**, *2* (4), a001040.
(37) Kondoh, H.; Lleonart, M. E.; Nakashima, Y.; Yokode, M.; Tanaka, M.; Bernard, D.; Gil, J.; Beach, D. A high glycolytic flux supports the proliferative potential of murine embryonic stem cells. *Antioxid. Redox Signaling* **2007**, *9* (3), 293−299.
(38) Robles, S. J.; Adami, G. R. Agents that cause DNA double strand breaks lead to p16INK4a enrichment and the premature senescence of normal fibroblasts. *Oncogene* **1998**, *16* (9), 1113−23.
(39) Leong, W. F.; Chau, J. F.; Li, B. p53 Deficiency leads to compensatory up-regulation of p16INK4a. *Mol. Cancer Res.* **2009**, *7* (3), 354−360.
(40) Itahana, Y.; Han, R.; Barbier, S.; Lei, Z.; Rozen, S.; Itahana, K. The uric acid transporter SLC2A9 is a direct target gene of the tumor suppressor p53 contributing to antioxidant defense. *Oncogene* **2014**, DOI: 10.1038/onc.2014.119.
(41) Ghneim, H. K.; Al-Sheikh, Y. A. The effect of aging and increasing ascorbate concentrations on respiratory chain activity in cultured human fibroblasts. *Cell Biochem. Funct.* **2010**, *28* (4), 283−292.
(42) Lushchak, O. V.; Piroddi, M.; Galli, F.; Lushchak, V. I. Aconitase post-translational modification as a key in linkage between Krebs cycle, iron homeostasis, redox signaling, and metabolism of reactive oxygen species. *Redox Rep.* **2014**, *19* (1), 8−15.
(43) (a) Mazurek, M. P.; Prasad, P. D.; Gopal, E.; Fraser, S. P.; Bolt, L.; Rizaner, N.; Palmer, C. P.; Foster, C. S.; Palmieri, F.; Ganapathy, V.; Stuhmer, W.; Djamgoz, M. B.; Mycielska, M. E. Molecular origin of plasma membrane citrate transporter in human prostate epithelial cells. *EMBO Rep.* **2010**, *11* (6), 431−437. (b) Mycielska, M. E.; Patel, A.; Rizaner, N.; Mazurek, M. P.; Keun, H.; Ganapathy, V.; Djamgoz, M. B. Citrate transport and metabolism in mammalian cells: prostate epithelial cells and prostate cancer. *Bioessays* **2009**, *31* (1), 10−20.
(44) Pitiyage, G. N.; Lim, K. P.; Gemenitzidis, E.; Teh, M. T.; Waseem, A.; Prime, S. S.; Tilakaratne, W. M.; Fortune, F.; Parkinson, E. K. Increased secretion of tissue inhibitors of metalloproteinases 1 and 2 (TIMPs −1 and −2) in fibroblasts are early indicators of oral sub-mucous fibrosis and ageing. *J. Oral Pathol. Med.* **2012**, *41* (6), 454−462.
(45) Yan, L. J.; Levine, R. L.; Sohal, R. S. Oxidative damage during aging targets mitochondrial aconitase. *Proc. Natl. Acad. Sci. U. S. A.* **1997**, *94* (21), 11168−11172.
(46) Zahavi, M.; Tahori, A. S. Citric acid accumulation with age in houseflies and other Diptera. *J. Insect Physiol.* **1965**, *11* (6), 811−816.
(47) Dominici, F. P.; Hauck, S.; Argentino, D. P.; Bartke, A.; Turyn, D. Increased insulin sensitivity and upregulation of insulin receptor, insulin receptor substrate (IRS)-1 and IRS-2 in liver of Ames dwarf mice. *J. Endocrinol.* **2002**, *173* (1), 81−94.
(48) Guarente, L.; Kenyon, C. Genetic pathways that regulate ageing in model organisms. *Nature* **2000**, *408* (6809), 255−262.
(49) Dai, D. F.; Rabinovitch, P. S.; Ungvari, Z. Mitochondria and cardiovascular aging. *Circ. Res.* **2012**, *110* (8), 1109−1124.
(50) Rizza, S.; Copetti, M.; Rossi, C.; Cianfarani, M. A.; Zucchelli, M.; Luzi, A.; Pecchioli, C.; Porzio, O.; Di Cola, G.; Urbani, A.; Pellegrini, F.; Federici, M. Metabolomics signature improves the prediction of cardiovascular events in elderly subjects. *Atherosclerosis* **2014**, *232* (2), 260−264.
(51) Schwarz, M. J.; Guillemin, G. J.; Teipel, S. J.; Buerger, K.; Hampel, H. Increased 3-hydroxykynurenine serum concentrations differentiate Alzheimer's disease patients from controls. *Eur. Arch. Psychiatry Clin. Neurosci.* **2013**, *263* (4), 345−352.
(52) Zwilling, D.; Huang, S. Y.; Sathyasaikumar, K. V.; Notarangelo, F. M.; Guidetti, P.; Wu, H. Q.; Lee, J.; Truong, J.; Andrews-Zwilling, Y.; Hsieh, E. W.; Louie, J. Y.; Wu, T.; Scearce-Levie, K.; Patrick, C.; Adame, A.; Giorgini, F.; Moussaoui, S.; Laue, G.; Rassoulpour, A.; Flik, G.; Huang, Y.; Muchowski, J. M.; Masliah, E.; Schwarcz, R.; Muchowski, P. J. Kynurenine 3-monooxygenase inhibition in blood ameliorates neurodegeneration. *Cell* **2011**, *145* (6), 863−874.
(53) Axelson, M.; Mork, B.; Aly, A.; Wisen, O.; Sjovall, J. Concentrations of cholestenoic acids in plasma from patients with liver disease. *J. Lipid Res.* **1989**, *30* (12), 1877−1882.
(54) Wiemann, S. U.; Satyanarayana, A.; Tsahuridu, M.; Tillmann, H. L.; Zender, L.; Klempnauer, J.; Flemming, P.; Franco, S.; Blasco, M. A.; Manns, M. P.; Rudolph, K. L. Hepatocyte telomere shortening and senescence are general markers of human liver cirrhosis. *FASEB J.* **2002**, *16* (9), 935−942.
(55) (a) Capparelli, C.; Guido, C.; Whitaker-Menezes, D.; Bonuccelli, G.; Balliet, R.; Pestell, T. G.; Goldberg, A. F.; Pestell, R. G.; Howell, A.; Sneddon, S.; Birbe, R.; Tsirigos, A.; Martinez-Outschoorn, U.; Sotgia, F.; Lisanti, M. P. Autophagy and senescence in cancer-associated fibroblasts metabolically supports tumor growth and metastasis via glycolysis and ketone production. *Cell Cycle* **2012**, *11* (12), 2285−2302. (b) Hassona, Y.; Cirillo, N.; Lim, K. P.; Herman, A.; Mellone, M.; Thomas, G. J.; Pitiyage, G. N.; Parkinson, E. K.; Prime, S. S. Progression of genotype-specific oral cancer leads to senescence of cancer-associated fibroblasts and is mediated by oxidative stress and TGF-beta. *Carcinogenesis* **2013**, *34* (6), 1286−1295.
(56) Jurk, D.; Wilson, C.; Passos, J. F.; Oakley, F.; Correia-Melo, C.; Greaves, L.; Saretzki, G.; Fox, C.; Lawless, C.; Anderson, R.; Hewitt, G.; Pender, S. L.; Fullard, N.; Nelson, G.; Mann, J.; van de Sluis, B.; Mann, D. A.; von Zglinicki, T. Chronic inflammation induces telomere dysfunction and accelerates ageing in mice. *Nat. Commun.* **2014**, *2*, 4172.

DOI: 10.1021/pr501221g
J. Proteome Res. 2015, 14, 1854−1871

(57) Castro, P.; Giri, D.; Lamb, D.; Ittmann, M. Cellular senescence in the pathogenesis of benign prostatic hyperplasia. *Prostate* **2003**, *55* (1), 30−38.
(58) Mycielska, M. E.; Broke-Smith, T. P.; Palmer, C. P.; Beckerman, R.; Nastos, T.; Erguler, K.; Djamgoz, M. B. Citrate enhances in vitro metastatic behaviours of PC-3M human prostate cancer cells: status of endogenous citrate and dependence on aconitase and fatty acid synthase. *Int. J. Biochem. Cell Biol.* **2006**, *38* (10), 1766−1777.

DOI: 10.1021/pr501221g
J. Proteome Res. 2015, 14, 1854−1871